Spectroscopic studies of the interaction of aluminum(III) with transferrins

James M. Aramini, Jillian A. Saponja, Hans J. Vogel *

Department of Biological Sciences, University of Calgary, Calgary, Alberta T2N 1N4, Canada

Contents

*Corresponding author.

Abstract

In this review, we summarize the spectroscopic techniques used to examine the binding of aluminum to the transferrins, a class of vertebrate iron-binding proteins. Interest in the binding of Al^{3+} by the transferrins, in particular serum transferrin, stems from the suggested role of metal detoxification in plasma by this protein and the association of this metal ion in human disorders such as Alzheimer's disease. A number of indirect methods of observing the binding of Al^{3+} to the transferrins, such as UV-visible spectroscopy, X-ray solution scattering, and ^1H and ^{13}C nuclear magnetic resonance (NMR) spectroscopy, have revealed information on the coordination and structure of the metal ion binding sites as well as conformational changes that occur on the binding of metal ions. Various NMR approaches, including ^{27}Al NMR, have elucidated subtle differences within the binding sites and between several transferrins. Most notably, the recent detection of transferrin-bound ^{27}Al NMR signals, characteristic of quadrupolar relaxation in the limit of slow molecular motion, has allowed us to observe directly the metal ion bound to the protein.

Keywords: Aluminium; Transferrins; Spectroscopy; Nuclear magnetic resonance; Quadrupolar central transition

List of abbreviations

acac	acetylacetonato
DNA	deoxyribonucleic acid
lTf	lactoferrin
lTf/2N	*N*-terminal half-molecule of lactoferrin
OTf	ovotransferrin
OTf/2C	*C*-terminal half-molecule of ovotransferrin
OTf/2N	*N*-terminal half-molecule of ovotransferrin
sTf	serotransferrin or serum transferrin
sTf/2N	*N*-terminal half-molecule of serotransferrin

1. Introduction

1.1. Transferrins

Transferrins are a family of large (molecular weight (MW), about 80 kDa) non-heme iron-binding glycoproteins that are of vital importance to the transport and homeostasis of iron in vertebrates (for recent reviews see Ref. [1]). Three major types of transferrins have been characterized: serotransferrin (sTf), a key serum protein which serves as a shuttle for metabolic iron, ovotransferrin (OTf), found in avian egg white, and lactoferrin (lTf), present in milk and other secretory fluids. The last two are thought to provide defense against bacterial infection. Transferrins are bilobal monomers, with each lobe containing one Fe^{3+}-binding site. Lobes within the same molecule and in different types of transferrins display strikingly high

sequence homologies [2], and it is widely accepted that transferrins evolved by gene duplication from a primordial protein [3]. The metal ion binding sites chelate high spin Fe^{3+} with remarkably high affinity ($K_D \approx 10^{-22}$ M), yet at the same time reversibly. In order to attain such traits, nature has designed an elegant system that is unique to transferrins, in which an anion (in vivo, carbonate) is both required and directly involved in the metal binding process. Neither the metal ion nor anion binds to these proteins with high affinity in the absence of the other, and hence the term "synergistic anion" was coined to describe the role of the latter. A number of other anions (for example, oxalate) may also fulfill the role of carbonate in vitro. Several years ago, it was postulated that the synergistic anion must possess a carboxylate moiety flanked by a second electron donor group, and that it both directly binds to the metal ion and interacts with basic protein residue(s) in the site (the "interlocking sites" model [4]). The high affinity Fe^{3+}-binding sites of transferrins also exhibit a rather broad metal ion specificity, illustrated by the number of diverse metal ions ranging in both charge and size that can bind to these proteins. This, together with the view that transferrins are not fully saturated with Fe^{3+} in vivo, raises the interesting possibility that these proteins could play a role in detoxification.

In the last two decades, a much more lucid picture of the nature and properties of the metal ion binding sites in transferrins has been obtained by a variety of spectroscopic techniques, including UV–visible spectrophotometry, electron spin resonance (ESR) spectroscopy, nuclear magnetic resonance (NMR) spectroscopy (for a recent review see Ref. [5]), and X-ray techniques. Such approaches have, for instance, revealed the existence of a direct bond between the synergistic anion and the bound metal ion, uncovered subtle differences in the environment and behavior of the metal ion binding sites within the same protein and/or different transferrins, and other factors that affect metal ion binding to these proteins, such as pH and the presence of non-synergistic anions. The recent flurry of X-ray crystallographic reports on several transferrins has shed considerable light on the structural aspects of the metal ion binding sites in transferrins. Studies on the Fe^{3+}-carbonate forms of human lactoferrin [6,7] and its recombinant *N*-terminal half-molecule, lTf/2N [8] have established that the high affinity iron-binding sites are situated in deep (about 10 Å) interdomain clefts in both lobes of the molecule. The metal ion is bound in a ternary complex to carbonate (bidentate) and the side chains of four highly conserved residues: 1 Asp, 1 His, and 2 Tyr (Fig. 1). The six ligands (five oxygen atoms and one nitrogen atom) are distributed around the metal ion in a distorted octahedral geometry. In both lobes the iron-binding residues originate from very different parts of the amino acid sequence; one from each domain (Asp, I; Tyr, II) and the others from two short interdomain strands. The bound carbonate lies in close proximity to the positively charged guanidinium group of an arginine and the *N*-terminus of an α-helix. Very similar results have been obtained for rabbit sTf and sTf/2N [10,11], and chicken OTf/2N [12]. In the intact proteins, the bound ferric ions are about 42 Å apart. Also, complementary helices in the lobes interact, fixing the relative orientation of the lobes; this may have implications regarding the ability of transferrins to recognize membrane-bound receptors which mediate the delivery of Fe^{3+} to the cell. Experiments with human apo-lTf have established that significant conforma-
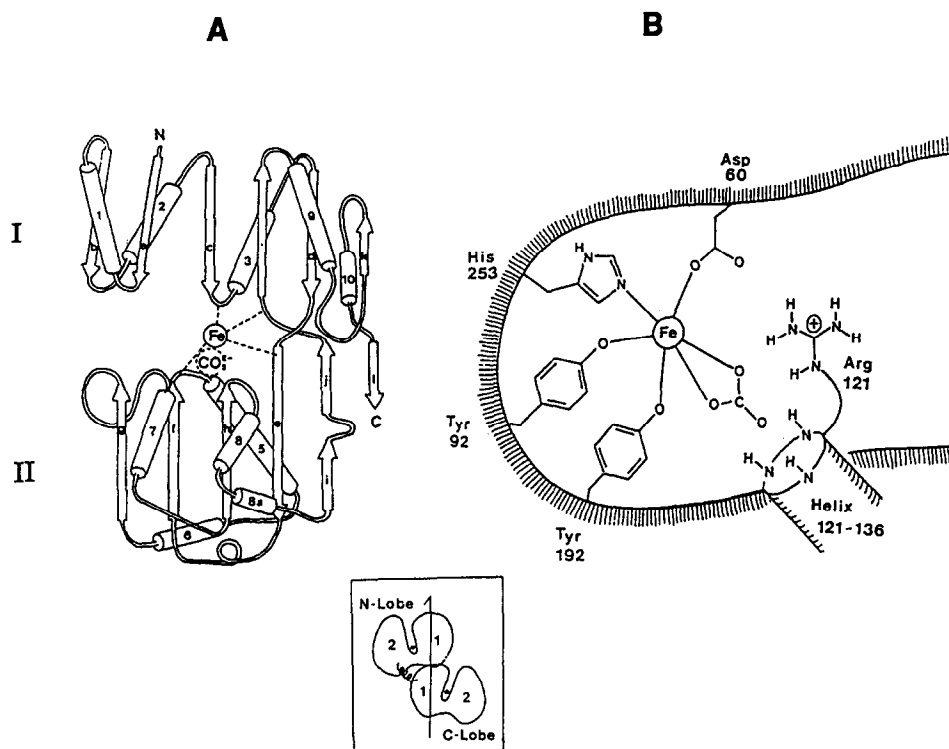
A   **B**

Fig. 1. (a) Structure of the recombinant N-terminal half-molecule of human lTf. Regions of secondary structure are represented by cylinders (α-helices) and arrows (β-strands). The domains are labeled with Roman numerals, and the bonds between the metal ion and protein residues are indicated by broken lines. (Reproduced with permission of Academic Press from Ref. [8].) (b) Schematic drawing of the Fe^{3+}-binding site in the N-lobe of human lTf. (Reproduced with permission of Academic Press from Ref. [7].) A cartoon of the ferrated intact protein is also shown. (Reproduced with permission of Elsevier Trends Journals from Ref. [9].)

tional changes occur during the transition between the apo- ("open") and holo- ("closed") forms of the protein, which are depicted in Fig. 2 [13,14]. From this work a "Venus fly-trap model" for metal ion binding in transferrins has been postulated, in which the two domains in each lobe move as rigid bodies about two pivot points located in the interdomain strands. X-ray solution scattering studies on several transferrins have corroborated this view [15–17]. Furthermore, X-ray crystal data for oxalate bound to Cu^{2+} in the C-terminal site of intact human lTf showed that this larger anion binds in a 1,2-bidentate fashion, leading to a modification in the interlocking sites model [18,19]. Very recent findings on a proteolytic fragment from duck OTf have given further insight into the mechanism of the metal ion binding process [20]. It is currently believed that anion binding is the first stage of the reaction, followed by metal ion binding to the two tyrosines in the site. The site is then snapped shut by the binding of the aspartate to the metal ion.
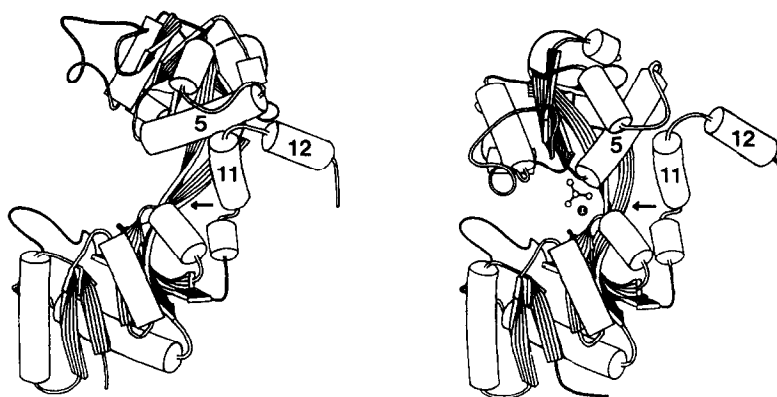
Fig. 2. Schematic representation of the N-lobe of human lTf, showing the conformational change between (a) open and (b) closed forms of the protein. Both Fe^{3+} and carbonate are shown in the closed form. An arrow marks the approximate hinge points in the interdomain strands. (Reproduced with permission of Macmillan Magazines from Ref. [13].)

Although much has been learned about the structures and properties of transferrins in recent years, questions concerning the biological action of these metalloproteins and in particular the nature of the transferrin-receptor interaction continue to linger.

1.2. Aluminum in biology

In vivo, transferrins are thought to be only partially saturated with ferric ion (about 30%) and this, together with their propensity for binding a variety of metal ions, has fueled speculation regarding a possible role for these proteins in the chelation and removal of toxic metal ions, such as Al^{3+}. Although aluminum has no known biological function, a toxic amount of Al^{3+} can cause dialysis encephalopathy in humans and is associated with other degenerative disorders such as senile dementia of the Alzheimer's type (see articles in Ref. [21]). Aluminum's role, if any, in Alzheimer's disease remains very controversial. In the early 1990s one radioisotope tracer (^{67}Ga) study provided evidence suggesting that sTf from people afflicted with Alzheimer's disease may be deficient in its ability to complex and remove Al^{3+}, contributing to the deposition of high levels of this metal in the brain [22]. The results of this work and the researchers' hypothesis have since been discredited [23,24]. A more recent article calls into question whether or not Al^{3+} is even present in the cerebral plaques of Alzheimer's patients and, hence, its suitability as a marker in the diagnosis of this ailment [25]; this has also been recently challenged by the discovery of an in vitro interaction between Al^{3+} and β-amyloid, a protein also deposited in the brain and postulated to play a key role in the etiology of the disease [26].

The questions regarding the toxicity of Al^{3+} plus the notion that transferrins, in particular sTf, play an important role in sequestering this metal ion [27] have spurred interest in the medically relevant aluminum derivatives of these proteins. In

this paper, we provide a survey of the spectroscopic approaches used to investigate the interactions of Al^{3+} with transferrins.

2. Spectroscopic studies of Al^{3+} binding in transferrins

2.1. Overview

The comparable six-coordinate ionic radii of Al^{3+} and high spin Fe^{3+} (0.54 vs. 0.65 Å [28]), make the former a suitable probe for the high affinity Fe^{3+}-binding sites of transferrins. However, the lack of both unpaired electrons and d electrons in Al^{3+} renders this metal ion undetectable by ESR and optical techniques, and essentially restricts the options for the direct spectroscopic observation of this diamagnetic metal ion in complexes to ^{27}Al NMR (notwithstanding X-ray crystallography). In addition to ^{27}Al NMR, researchers in the transferrin field have employed a number of indirect methods to study Al^{3+} binding to these proteins; these techniques involve the detection of protein ligands (i.e. UV–visible spectrophotometry), the anion (i.e. ^{13}C NMR), and conformational changes in the protein (i.e. X-ray solution scattering and ^{1}H NMR) resulting from metal ion binding. Recent applications of each of the five approaches introduced in this section to the study of the interaction of Al^{3+} with transferrins will be discussed in turn below.

2.2. Use of transferrin half-molecules

Prior to reviewing the spectroscopic techniques that have been successfully applied to the investigation of Al^{3+} binding to transferrins, we discuss a common and effective assignment strategy employed by spectroscopists in this field, namely the use of transferrin half-molecules. There are two approaches generally used for the production of intact, functional transferrin half-molecules: (1) proteolysis and (2) recombinant DNA technology.

In our work with chicken OTf, we employ a protocol introduced by Oe et al. [29] to generate and purify the *N*- and *C*-terminal half-molecules of this protein (OTf/2N and OTf/2C). In this approach, diferric OTf is mildly digested with trypsin, which cleaves the linker between the two lobes of the protein, affording half-molecules approximately 36 (N) and 40 (C) kDa in size (Fig. 3). The *N*-terminal half-molecule of chicken OTf may also be isolated according to the method of Nakazato et al. [30], which exploits the preferential binding of Al^{3+} to the *N*-terminal site of this protein (vide infra). In this procedure the apoprotein, in the presence of carbonate, is selectively loaded with Al^{3+} in its N-lobe, and the exposed *C*-terminal lobe of the protein is digested away with trypsin. Analogous protocols for the synthesis of half-molecules from human sTf and human lTf have also been reported (i.e. Refs. [31,32]). The OTf half-molecules generated by these schemes can be purified chromatographically and assigned on the basis of their carbohydrate content using a sensitive periodate–Schiff (PAS) assay [33]. Note that only the *C*-lobe in chicken OTf (and human sTf, vide infra) is glycosylated; both lobes are glycosylated in human lTf
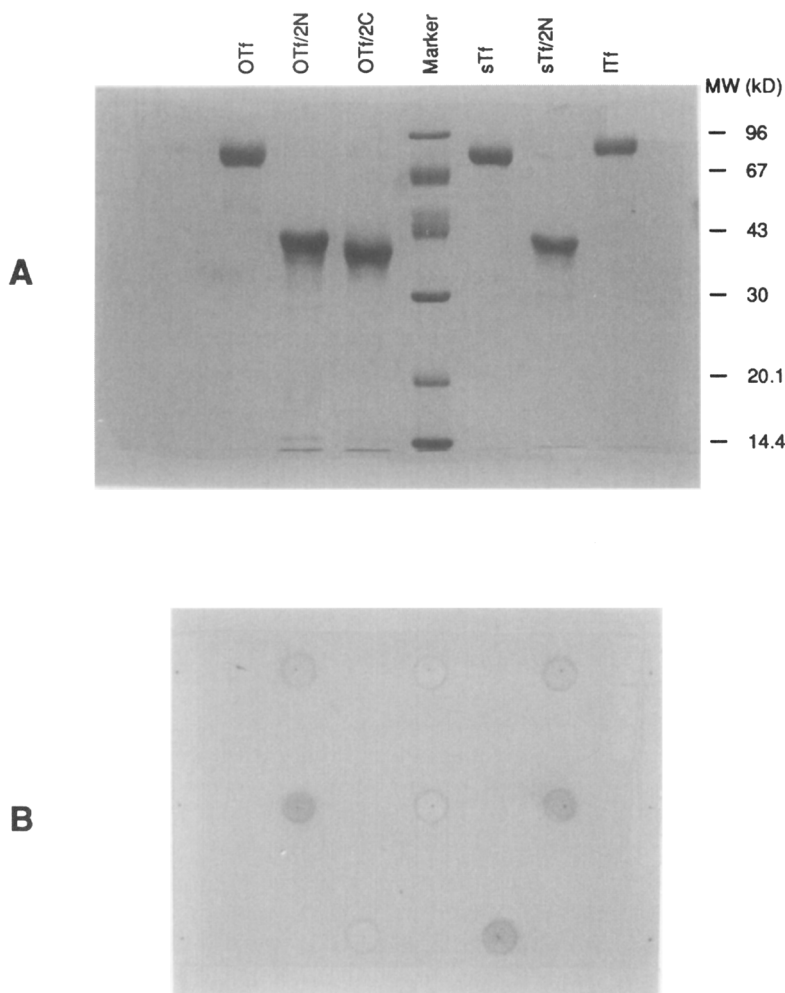
Fig. 3. (a) 12% sodium dodecyl sulfate–polyacrylamide gel electrophoresis and (b) PAS assay (bottom) of the transferrins studied in our laboratory. In the PAS assay, a faint circle indicates the position of each blot: top row (left to right), OTf (+), OTf/2N (−), OTf/2C (+); middle row (left to right), human sTf (+), recombinant sTf/2N (−), human lTf (+); bottom row (controls), α-lactalbumin (−); ovalbumin (+; right). (J.M. Aramini and H.J. Vogel, unpublished results.)

(Ref. [4] and references therein). In this assay, a small amount of protein (2–5 μl of a 0.1–1 mM solution) is blotted onto nitrocellulose paper, and treated with Schiff's reagent. Blots containing glycosylated protein appear as pink spots. Fig. 3 also shows a photograph of a PAS assay on some of the transferrins and half-molecules used in our work.

In recent years, methods for the expression of transferrin half-molecules have been introduced. We will show below how NMR spectroscopists have made use of the

recombinant 40 kDa N-terminal half-molecule of human sTf (sTf/2N), expressed in large quantities in baby hamster kidney cells and purified as described by Funk et al. [34] and Mason et al. [35]. As with the corresponding lobe in the parent protein, this molecule is devoid of covalently bound oligosaccharides (Fig. 3). An analogous expression system has recently been developed for the N-terminal half-molecule of human lTf [36]. Although technically demanding, this methodology has its advantages over proteolytic approaches, especially in terms of the homogeneity of the final product.

From our experience with transferrins, we believe that the method of choice to assign spectroscopic data for these proteins is the use of the half-molecules described in this section, which contain the intact binding sites. We feel that the half-molecule approach is superior to previous methods which have exploited the differences in the binding properties of the sites in these proteins to generate mixed derivatives with Fe^{3+} specifically loaded into one site of the protein and the metal ion of interest in the other (i.e. Refs. [37,38]). Recall that the selectivity of iron binding in transferrins is dependent on a host of factors, such as pH, secondary anions, and the metal ion complex [1c]. Hence, it is not surprising that the latter approach can be perilous for assignment purposes, and in some instances the half-molecule methodology has overturned earlier incorrect assignments [39].

2.3. Difference UV spectrophotometry

UV–visible spectrophotometry has over the years proven to be one of the most commonly used spectroscopic techniques for evaluating the interaction of transferrins with a wide variety of metal ions [1c], and Al^{3+} is no exception. Two recent reports of the application of this approach to the study of Al^{3+} binding to human sTf [40] and chicken OTf [41] are discussed in this section.

Harris and Sheldon [40] used difference UV spectrophotometry to analyze the binding of Al^{3+} to human sTf. When titrating the apoprotein with this metal ion, these researchers observed absorbance maxima at wavelengths of 240 and 288 nm, due to the tyrosines which participate in metal ion binding in both sites (Fig. 4); this pattern is quite diagnostic of metal ion binding in transferrins. Using the change $\Delta\varepsilon$ in absorptivity of the more intense band ($\lambda = 240$ nm) as a function of titrant added, they deduced that Al^{3+} binding proceeds sequentially and obtained apparent Al^{3+} affinity constants for the sites ($\log K^* = 13.5$ and 12.5). Using monoferric forms of sTf, in which Fe^{3+} is selectively loaded into one of the two sites of the protein, they assigned the larger binding constant to the C-terminal site, thus concluding that the metal ion binds preferentially at this site. Interestingly, in their titration experiments, Harris and Sheldon found a leveling off of $\Delta\varepsilon$ prior to two equivalents of Al^{3+} and ascribed this failure to reach saturation to a competition reaction involving hydroxide ion, leading to the formation of $Al(OH)_3$. In previous UV titration studies of Al^{3+} binding to human sTf, affinity constants in the range $\log K^* \approx 12$–15.5 were reported [42,43].

In an analogous difference UV study of the binding of a host of metal ions to chicken OTf, Ichimura et al. [41] found that Al^{3+}, like Fe^{3+}, binds with an over-
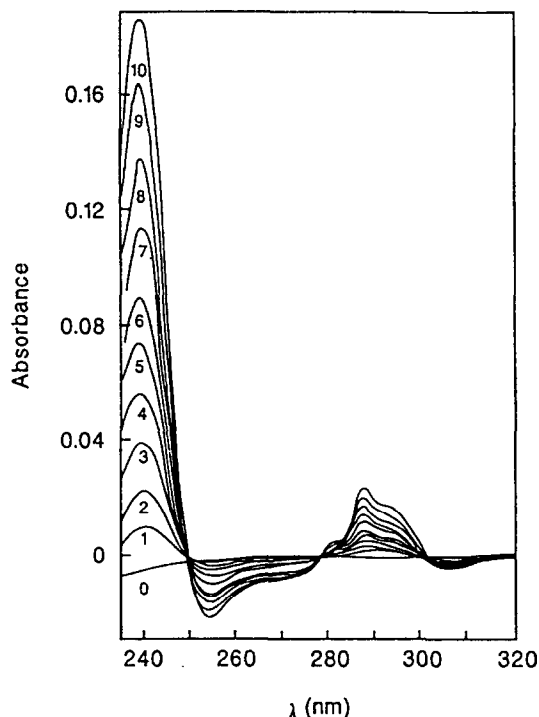
Fig. 4. Difference UV spectra of the titration of human apo-sTf (8.34 μM) with Al^{3+} (0.220 mM) for various volumes of Al^{3+} stock solution added: spectrum 0, 0 μl; spectrum 1, 10 μl; spectrum 2, 20 μl; spectrum 3, 30 μl; spectrum 4, 40 μl; spectrum 5, 50 μl; spectrum 6, 65 μl; spectrum 7, 85 μl; spectrum 8, 105 μl; spectrum 9, 125 μl; spectrum 10, 155 μl. (Reproduced with permission of the American Chemical Society from Ref. [40].)

whelming preference for the N-terminal site of the protein and reported a ratio K_C/K_N of affinity constants for the sites of 0.12. Moreover, they reported that Al^{3+} binding to this protein is characterized by negative cooperativity, in stark contrast to Fe^{3+}.

2.4. X-ray solution scattering

X-ray solution scattering is an established spectroscopic technique that is well suited for probing the overall size and conformation of biological macromolecules in solution [44]. Grossmann et al. recently employed this methodology to investigate conformational changes in chicken OTf resulting from the binding of several metal ions, including Al^{3+} [16]. They found that the binding of certain metal ions, such as In^{3+} and Cu^{2+}, caused a marked reduction in the radius R_g of gyration, a measure of the overall size of the molecule, similar in magnitude to what was observed earlier for the native metal ion, Fe^{3+} [15] (Table 1). It was reasoned that such metal ions mediate a change in conformation in both lobes of the protein from an "open" (apo)

Table 1
Radii of gyration for various metal ion bound forms of chicken OTf

M^{x+}	Ionic radius[a] (Å)	R_g[b] (Å)
Fe^{3+}	0.65	29.7
Cu^{2+}	0.73	29.9
In^{3+}	0.80	29.9
Al^{3+}	0.54	30.1
Hf^{4+}	0.71	30.4
apo	—	30.5

[a] Six-coordinate ionic radii obtained from Ref. [28].
[b] Data obtained from Ref. [16].

to a "closed" (holo) form. Actinides, such as Hf^{4+}, cause no perturbation in R_g, indicative of a lack of strong interaction with the protein, which remains in the open conformation. However, although it exhibits a high affinity for the metal ion binding sites in transferrins, Al^{3+} causes only a moderate conformational change, indicated by an R_g intermediate between those observed for other strongly bound metal ions (closed form) and the apoprotein (open form). Grossmann et al. suggest that this effect may be attributable to the small ionic radius of Al^{3+} and its propensity for forming six-coordinate complexes. They hypothesize that Al^{3+} binding may cause significant movement of one or more protein ligands in order to accommodate the small cation; this would result in a disruption of the interdomain hydrogen-bonding network within each lobe, compared with that observed with Fe^{3+} [8], and a concomitant decrease in interdomain closure, leading to a less compact overall structure.

Grossmann et al. suggest that their findings have ramifications concerning the fate of Al^{3+} in vivo, in particular the route by which it enters brain cells. Cell surface transferrin receptors, involved in the receptor-mediated endocytotic acquisition of iron by cells, exhibit an appreciably higher affinity for the diferric form of the protein compared with the apoprotein [45]. Hence, because its overall conformation is not equivalent to diferric sTf, the Al^{3+}—sTf complex should be easily discriminated by transferrin receptors.

2.5. ^1H nuclear magnetic resonance spectroscopy

With the advent of high field magnets and sophisticated multidimensional pulse techniques, ^1H NMR spectroscopy has become the focal point of a powerful tool for gaining insights into the structures and dynamics of small (up to about 20 kDa) biologically important macromolecules in solution (for recent treatises on this subject see Ref. [46]). However, appreciable signal overlap combined with decreased signal resolution due to line broadening severely hamper the application of this technique for proteins the size of transferrins. Nevertheless, several groups have very recently used one- and two-dimensional ^1H (500 MHz) NMR spectroscopy to monitor Al^{3+} binding to human sTf and its recombinant N-terminal half-molecule [47,48]. Their

approach hinges on the detection of conformational changes in the protein associated with metal ion binding and on the use of resolution enhancement techniques during data processing, which retain the relatively sharp peaks due to protons in more mobile parts of the protein. They found that individual signals, namely His C2H protons in the aromatic region of the spectrum ($\delta \approx 7.5$–8.0 ppm) and ring-current-(upfield)-shifted aliphatic protons ($\delta \approx 0$ to -1 ppm), can be resolved in the one-dimensional ^{1}H NMR spectrum. The latter is particularly sensitive to conformational changes in proteins, typified by the large domain movements which accompany metal ion binding in transferrins. Spectra of the Al^{3+} titrations of recombinant sTf/2N and native sTf, showing only the upfield-shifted aliphatic region, are shown in Fig. 5 [47b]. For both proteins, Al^{3+} binding results in a decrease in the signals due to the apoprotein and a simultaneous appearance of a new set of signals, an effect characteristic of slow exchange binding of the metal ion to each molecule. An example of this is signal B, which Kubal et al. tentatively assigned by two-dimensional ^{1}H NMR and modeling to a δ-methyl group in a Leu (122); this resonance moves about 0.06 ppm upfield on addition of Al^{3+} (B'). Similar effects were noted in the His C2H region of the spectrum. In their initial experiments with the intact protein, these researchers found that Al^{3+} binding occurs sequentially in the protein, with
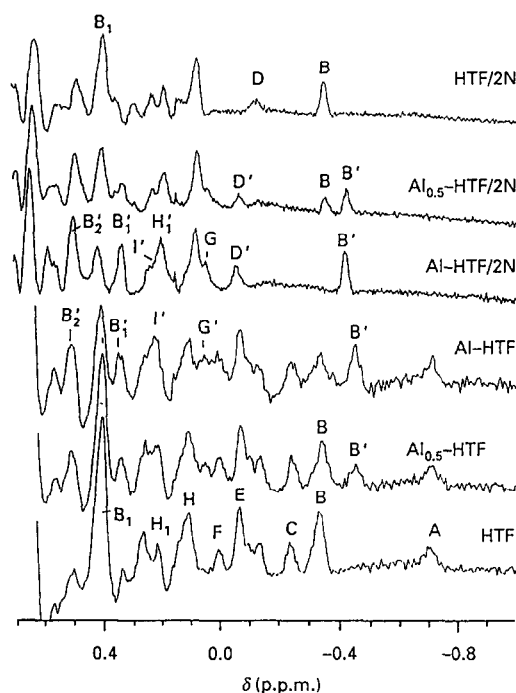

Fig. 5. The upfield-shifted aliphatic regions of resolution-enhanced ^{1}H (500 MHz) NMR spectra of the titrations of human sTf and its recombinant N-terminal half-molecule with Al^{3+}. The peaks have been labeled with a prime for the Al^{3+} complex to illustrate the correspondence in features between the two proteins. (Reproduced with permission of Portland Press from Ref. [47b].)

one set of peaks diagnostic of the binding of the first equivalent of metal ion and a second set of signals corresponding to the second equivalent [47a]. Their subsequent experiments on the half-molecule depicted in Fig. 5 established that Al^{3+} is bound preferentially at the *N*-terminal site of the protein, since near-identical results were obtained with both sTf and sTf/2N in the first half of the titration. These experiments refute the site preference reported above by Harris and Sheldon [40], and Kubal et al. postulate that the binding of Al^{3+} at the *N*-lobe is the kinetically favored product. These groups have since extended their technique to the study of Ga^{3+} and In^{3+} binding to human sTf [48,49].

2.6. ^{13}C nuclear magnetic resonance spectroscopy

In addition to serving as a direct probe of the anion binding sites in transferrins, the use of ^{13}C NMR to monitor the concomitant binding of a ^{13}C-enriched anion, such as carbonate or oxalate, to transferrins is yet another well-established indirect spectroscopic approach to investigating the binding of numerous diamagnetic metal ions to these proteins [5]. Two groups, Bertini et al. [50] and our group (i.e. Refs. [51,52]), have applied this methodology to the study of Al^{3+} binding to several transferrins in the presence of both ^{13}C-enriched carbonate and ^{13}C-enriched oxalate.

2.6.1. Experiments with carbonate

The bulk of the applications of this methodology to transferrins have involved the use of ^{13}C-labeled carbonate. Fig. 6 shows the Al^{3+} titration of human apo-sTf in the presence of an excess of labeled carbonate followed by ^{13}C (and ^{27}Al, vide infra) NMR at a magnetic field B_0 of 9.4T [53]. In the absence of Al^{3+}, one observes in the carbonyl region of the spectrum a sharp signal at $\delta = 161.1$ ppm due to the labeled anion (primarily bicarbonate at this pH) plus natural abundance ^{13}C resonances corresponding to backbone and side chain carbonyls ($\delta \approx 170$–183 ppm) and the guanidinium group of arginine residues ($\delta = 157.8$ ppm) in the protein. In addition, there is a signal at $\delta \approx 164.5$ ppm corresponding to the bound anion in the vacant metal ion binding site(s) of the apoprotein [54]. On addition of Al^{3+}, one observes two ^{13}C signals ($\delta = 166.16$ and 165.83 ppm) which increase in intensity up to two equivalents of metal ion, and the simultaneous disappearance of the signal at $\delta = 164.5$ ppm. On the basis of ^{13}C chemical shift and pH data and the refined X-ray structures of lTf and rabbit sTf/2N [7,11,50,54], it is generally accepted that these partially overlapping signals correspond to carbonate (not bicarbonate) bound in a ternary complex with Al^{3+} and sTf in each of the two Fe^{3+}-binding sites of this protein. When the experiment on the intact protein is conducted with added salt (i.e. 150 mM KCl), Al^{3+} binding proceeds sequentially, with the upfield resonance appearing prior to the other [53]. In analogous lower field ($B_0 = 7.0$ T) experiments performed by Bertini et al. [50] only one broad resonance was observed for the Al^{3+}–$^{13}CO_3^{2-}$ forms of both human sTf and chicken OTf (vide infra). The discrepancy with the findings in this work stems from the fact that the closely spaced resonances resulting from carbonate binding at each site could not be resolved at the magnetic field strength used in the earlier study. We have found similar overlapping signals
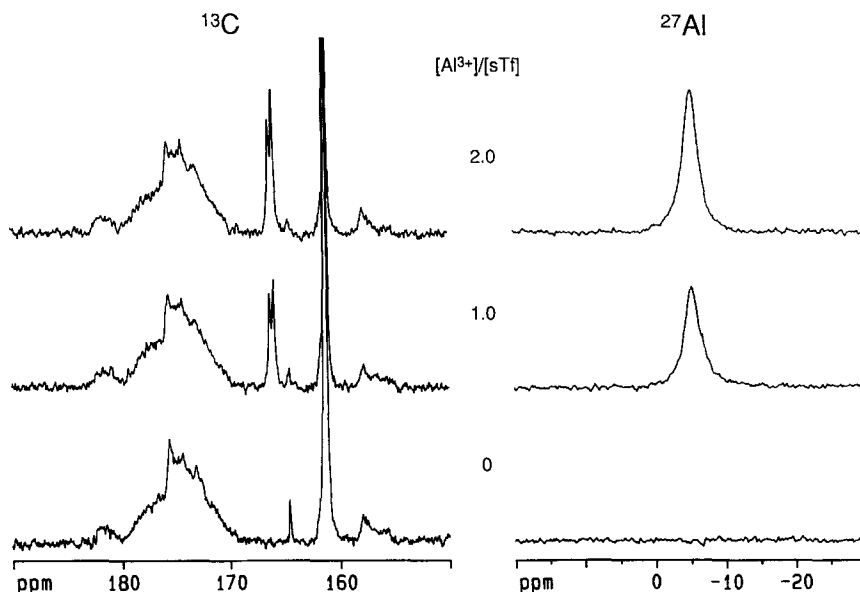
Fig. 6. ^{13}C (100.6 MHz) and ^{27}Al (104.3 MHz) NMR spectra of 1.09 mM sTf in the presence of 20 mM Na$_2$^{13}CO$_3$, no KCl, pH 7.5, and various amounts of Al^{3+}. ^{13}C: 20 000 scans each; only the carbonyl region of each spectrum is shown. ^{27}Al: 150 000 scans each [53].

in high field ($B_0 = 9.4$ and 11.7 T) ^{13}C NMR studies of other M^{3+}–^{13}CO$_3^{2-}$ adducts of the transferrins (i.e. M = Sc or Ga [55,56]).

The ^{13}C signals for this complex can be assigned to the Al^{3+}–^{13}CO$_3^{2-}$ form of the recombinant N-terminal lobe of sTf which gives a signal at exactly the same frequency as the upfield signal in the intact protein (Fig. 7). This means that, in the presence of added salt, Al^{3+} is bound preferentially at the N-lobe of human sTf, in agreement with the ^{1}H NMR findings discussed earlier.

The ^{13}C NMR methodology outlined above for human sTf can be extended to the Al^{3+}–^{13}CO$_3^{2-}$ forms of other transferrins. For example, in the case of chicken OTf, we again found two closely spaced ^{13}C signals at virtually identical points in the spectrum ($\delta = 165.73$ and 165.52 ppm), when the protein is saturated with Al^{3+} in the presence of ^{13}C-labeled carbonate (Fig. 8 [51,52]). In titration studies of this protein, we found that the signals appear sequentially on addition of Al^{3+}; specifically, when one equivalent of the metal ion is added to the apo-OTf the downfield peak $\delta = 165.73$ ppm emerges, with the other signal appearing on addition of a second equivalent of titrant [51].

The assignments of these signals were obtained by analyzing the isolated N- and C-terminal half-molecules of the protein (Fig. 8). Again, for the intact protein two overlapping resonances are observed corresponding to the binding of carbonate to each metal ion binding site in OTf. When a stoichiometric amount of Al^{3+} is added to OTf/2C in the presence of the same anion a signal appears at exactly the same chemical shift as the upfield peak in the intact molecule. In the case of OTf/2N only
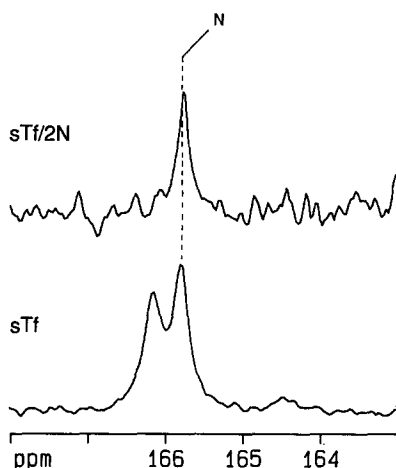
Fig. 7. ^{13}C (100.6 MHz) NMR spectra of the Al^{3+}–$^{13}CO_3^{2-}$ forms of sTf (1.09 mM, 2.0 equivalents Al^{3+}, pH 7.5, 20 000 scans) and sTf/2N (0.22 mM, 0.8 equivalents Al^{3+}, 0.10 M KCl, pH 7.6, 60 000 scans). For both spectra, only a narrow window of the carbonyl region is shown [53].
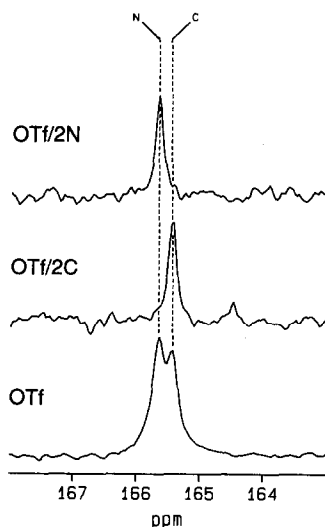

Fig. 8. ^{13}C (100.6 MHz) NMR spectra of the aluminum–carbonate derivatives of intact OTf and its half-molecules. OTf: 1.13 mM OTf, pH 7.6 20 000 scans. OTf/2C: 1.25 mM OTf/2C, pH 7.8, 20 000 scans. OTf/2N: 0.19 mM OTf/2N, pH 7.7, 60 000 scans. Only a narrow window of the carbonyl region of each spectrum is shown. (Reproduced with permission of the American Chemical Society from Ref. [51].)

the downfield resonance is observed. Taken together with the results from titration experiments, these assignments indicate that in the presence of carbonate the *N*-terminal site of OTf has a higher affinity for Al^{3+} than the C site, in agreement with the UV data of Ichimura et al. [41] alluded to above.
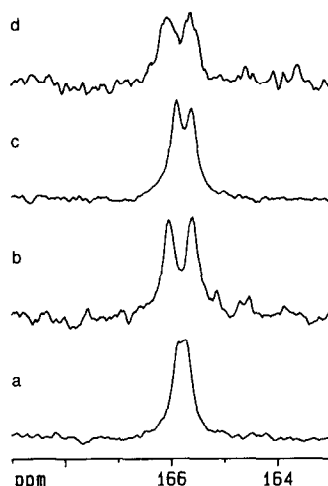
Fig. 9. ^{13}C (100.6 MHz) NMR spectra of the aluminum–carbonate adducts of several transferrins: spectrum a, turkey OTf (1.1 mM, pH 7.6, 20 000 scans); spectrum b, human lTf (0.73 mM, pH 7.5, 20 000 scans); spectrum c, bovine sTf (1.2 mM, pH 7.5, 20 000 scans); spectrum d, bovine lTf (0.38 mM, pH 7.6, 35 000 scans) [57].

^{13}C NMR spectra of four other transferrins (turkey OTf, human lTf, bovine sTf, and bovine lTf) in the presence of saturating and excess amounts of Al^{3+} and ^{13}C-enriched carbonate respectively are shown in Fig. 9 [57]. For each protein, one again observes two overlapping ^{13}C signals due to the anion bound to the metal ion and protein residues in the two high affinity metal ion binding sites. We found no evidence for site preference in titration experiments with all of these proteins. The ^{13}C data for the Al^{3+}–^{13}CO$_3^{2-}$ forms of the six transferrins discussed in this section are given in Table 2.

2.6.2. Experiments with oxalate

The ^{13}C NMR methods discussed above are also suited for analyzing the binding of non-biological synergistic anions, such as oxalate, to transferrins. Changing the synergistic anion from carbonate to the larger oxalate allows one to detect more easily subtle spectroscopic differences between pairs of metal ion–anion binding sites in the same transferrin molecule. For example, as shown in Fig. 10, when two equivalents of Al^{3+} are added to chicken apo-OTf in the presence of excess ^{13}C-labeled oxalate, two pairs of overlapping doublets (i.e. two AB spin systems) are observed upfield of free oxalate (a singlet at $\delta = 174.2$ ppm), corresponding to the carboxyl carbons of oxalate bound in a ternary complex to Al^{3+} and protein residues in both metal ion binding sites of the protein [51]. Very similar results for chicken OTf were first reported by Bertini et al. [50]. Originally, we and the Bertini group believed that this multiplet pattern could be best described by a model in which one carboxylate group from the oxalate binds in either a monodentate or a 1,1-bidentate

Table 2
^{13}C nuclear magnetic resonance data for the $Al^{3+}-{}^{13}CO_3^{2-}$ adducts of various transferrins

Protein	^{13}C δ (ppm)	Assignment[a]
Human sTf	166.16 [b]	C
	165.83 [b]	N
	165.4 [c]	N, C
Chicken OTf	165.73 [d]	N
	165.52 [d]	C
	165.9 [c]	N, C
Human lTf[b]	166.01	n.d.
	165.55	n.d.
Turkey lTf[b]	165.88	n.d.
	165.76	n.d.
Bovine sTf [b]	165.88	n.d.
	165.61	n.d.
Bovine lTf [b]	166.03	n.d.
	165.57	n.d.

[a] Obtained from experiments with OTf/2N, OTf/2C and sTf/2N; n.d. not determined.
[b] Data obtained from Ref. [57].
[c] Data obtained from Ref. [50].
[d] Data obtained from Refs. [51,52].

manner to the metal ion, leaving the other carboxylate to interact with basic residues in the binding cleft. However, several lines of spectroscopic evidence, including ^{205}Tl NMR [39], electron spin echo envelope modulation [58], and X-ray crystallography [19], strongly suggest that in several $M^{3+}-C_2O_4^{2-}$ adducts of transferrins this anion binds in a 1,2-bidentate fashion to the metal ion.

Analogous to the approaches used in the experiments involving carbonate, the complex pattern of ^{13}C signals observed for intact OTf can be deciphered with the use of the proteolytic half-molecules of the protein (Fig. 10). In the case of OTf/2C two doublets are observed, the second of which lines up well with the most upfield doublet detected for the intact protein. For OTf/2N, one again observes two doublets, of which the more upfield is quite distinct from that seen for OTf/2C. Note that the most downfield doublets for the two half-molecules resonate at slightly different frequencies in the half-molecules, and the spin–spin coupling constant $^1J(^{13}C-^{13}C)$ is slightly larger for oxalate bound to the N site (Table 3). In combination with titration experiments on this system, we determined from these assignments that, in the presence of oxalate, Al^{3+} binds with higher affinity at the C site of OTf. This site preference, although not as pronounced as that observed for carbonate [51], is opposite to that found for carbonate; this reflects a difference in the ability of the sites to accommodate anions of different size. A similar site preference (i.e. C > N) was recently reported for Ga^{3+} binding to human sTf in the presence of oxalate [49,56].

Analogous ^{13}C NMR experiments in our laboratory on other transferrins suggest that when oxalate acts as the synergistic anion Al^{3+} binding is sequential
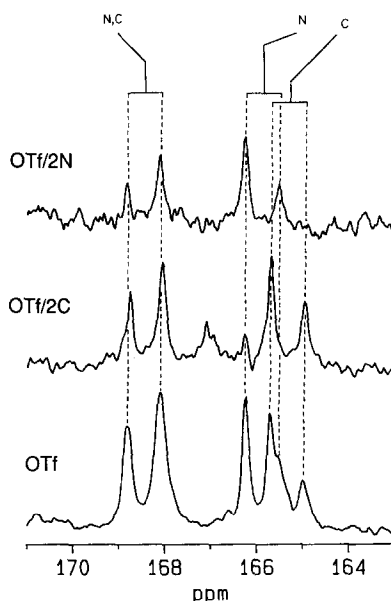
Fig. 10. ^{13}C (100.6 MHz) NMR spectra of the aluminum–oxalate derivatives of intact OTf and its half-molecules. OTf: 1.18 mM OTf, pH 7.5, 20 000 scans. OTf/2C: 0.72 mM OTf/2C, pH 7.4, 40 000 scans. OTf/2N: 0.18 mM OTf/2N, pH 7.7, 75 000 scans. Only a narrow window of the carbonyl region of each spectrum is shown. The peak at $\delta \approx 167$ ppm in the OTf/2C spectrum is an impurity that emerges in the preparation of this half-molecule after repeated recycling. (Reproduced with permission of the American Chemical Society from Ref. [51].)

Table 3
^{13}C nuclear magnetic resonance data for the Al^{3+}–$^{13}C_2O_4^{2-}$ adducts of various transferrins

Protein	$^{13}C_1$ δ (ppm)	$^{13}C_2$ δ (ppm)	$^1J(^{13}C-^{13}C)$ (Hz)	Site
Chicken OTf	168.47	165.89	73	N [a]
	168.42	165.33	70	C
	169.2	166.2	68	N [b]
	169.2	165.8	71	C
Human sTf [c]	168.58	166.07	75	n.d.
	168.40	165.33	73	n.d.
Human lTf [c]	168.55	166.0	73	n.d.
	168.24	166.0	70	n.d.

[a] Data obtained from Ref. [51]; assignments obtained from experiments with OTf/2N and OTf/2C.
[b] Data obtained from Ref. [50]; assignments were made on the basis of pH dependence.
[c] Data obtained from Ref. [57]; sites not assigned (n.d.).

in the case of human lTf (sites not assigned), but not for human sTf [57]. The ^{13}C NMR data for the Al^{3+}–oxalate forms of a number of transferrins are given in Table 3.

2.7. ^{27}Al nuclear magnetic resonance spectroscopy

2.7.1. Properties of ^{27}Al

As we mentioned earlier, ^{27}Al NMR spectroscopy is practically the only technique capable of directly observing this otherwise spectroscopically silent element. This nucleus, which is quadrupolar (i.e. has a nuclear spin I greater than $\frac{1}{2}$), possesses a number of favorable traits, listed in Table 4. ^{27}Al has a high natural abundance, good receptivity and a relatively small quadrupole moment; these properties make it quite amenable to study by NMR (for reviews see Ref. [59]).

From numerous ^{27}Al NMR studies of low molecular weight inorganic aluminum complexes in recent years, it has been established that the ^{27}Al chemical shift range spans about 300 ppm and that this parameter is indicative of the number of ligands involved in coordinating the metal ion [59a]. Despite the promise of this technique, the number of literature examples of the use of ^{27}Al NMR as a spectroscopic probe for the binding of Al^{3+} to proteins is relatively few [51,52,62–64].

A few important technical aspects concerning ^{27}Al NMR spectroscopy bear mentioning here. First, the presence of aluminum in the materials used to construct the probes employed in NMR spectroscopy causes a very broad ($\Delta v_{1/2} \approx 7$ kHz) resonance which can seriously hamper the detection of desired signals [59a], particularly at the concentrations generally used in protein work (about 1 mM). To circumvent this, we acquire ^{27}Al NMR spectra with dead times (the interval between the pulse and the start of acquisition) on the order of 250 µs; we find that this value for the dead time is required to attenuate the resonance effectively without appreciable loss of intensity for transferrin-bound ^{27}Al signals. In addition, all the ^{27}Al NMR chemical shifts reported in subsequent sections are with respect to external 1.0 M $Al(NO_3)_3$ in D_2O.

2.7.2. Quadrupolar relaxation theory

In order to have a grasp of the physical information regarding the nature of the metal ion binding sites in transferrins that can be gleaned from ^{27}Al NMR spectroscopy, it is pertinent to summarize briefly a few key aspects of quadrupolar relaxation.

In general, the dominant relaxation pathway for quadrupolar nuclei such as ^{27}Al is the quadrupolar relaxation mechanism, a process which involves an electric interaction between the nuclear quadrupole moment and fluctuating electric field gradients at the nucleus [65,66]. The electric field gradients originate from valence

Table 4
Nuclear magnetic resonance properties of ^{27}Al

I	a [a] (%)	γ [b] ($\times 10^7$ rad T^{-1} s^{-1})	v_0 (9.4 T) [b] (MHz)	R [b] (per ^{13}C)	Q [a] ($\times 10^{-28}$ m^2)
$\frac{5}{2}$	100	6.9704	104.3	1.17×10^3	0.140

[a] Natural abundance (a) and quadrupole moment (Q) taken from Ref. [60]. [b] Gyromagnetic ratio (γ), resonance frequency (v_0) and receptivity (R) taken from Ref. [61].

electrons in the vicinity of and directly involved in bonding to the element of interest. Under isotropic conditions (i.e. liquids), molecular tumbling modulates the interaction between the electric field gradient and the nucleus, providing an avenue for nuclear relaxation. Some time ago it was noted [67] that in this case the decays of the longitudinal and transverse magnetizations of a quadrupolar nucleus are described by the sum of I (if I is integer) or $I + \frac{1}{2}$ (if I is half-integer) exponentials, corresponding to allowed single-quantum ($\Delta m = \pm 1$) transitions between the $2I + 1$ nuclear Zeeman energy levels. For $I = \frac{5}{2}$ nuclei such as ^{27}Al the observed magnetization can be attributed to three components, where component I corresponds to the central ($m_I = \frac{1}{2} \to -\frac{1}{2}$) transition and the outer ($m_I = \frac{3}{2} \to \frac{1}{2}$, $m_I = -\frac{1}{2} \to -\frac{3}{2}$; $m_I = \frac{5}{2} \to \frac{3}{2}$, $m_I = -\frac{3}{2} \to -\frac{5}{2}$) transitions constitute components II and III respectively. The T_1 and T_2 relaxation rates for each component are critically dependent on the motion and frequency of the nucleus in question (i.e. $\omega_0 \tau_c$). For any quadrupolar nucleus relaxation can be subdivided into three windows of molecular motion: $\omega_0 \tau_c \ll 1$, $\omega_0 \tau_c \approx 1$, and $\omega_0 \tau_c \gg 1$. We discuss two of these below.

Extreme narrowing conditions ($\omega_0 \tau_c \ll 1$) For small molecules which tumble rapidly in solution, the relaxation rates of all components are identical and quadrupolar relaxation is characterized by a single exponential decay. The general expression for the relaxation times T_1 and T_2 for any $I > \frac{1}{2}$ nucleus is given by

$$\frac{1}{T_1} = \frac{1}{T_2} = \pi \, \Delta v_{1/2} = \frac{3\pi^2}{10} \frac{(2I + 3)}{I^2(2I - 1)} \chi^2 \tau_c \left(1 + \frac{\eta^2}{3}\right) \tag{1}$$

where χ, the quadrupole coupling constant, is a key parameter that provides a measure of the relative symmetry of the electric environment of the nucleus. This physical quantity will be discussed in more detail below. In addition, η, the asymmetry parameter, accounts for the deviation from cylindrical symmetry of the electric field gradient at the nucleus, and ranges from 0 to 1; in practice this entire term is usually neglected (in this and subsequent expressions). Note that under these conditions the signal linewidth $\Delta v_{1/2}$ is directly proportional to τ_c, and quadrupolar relaxation data give a product of χ and τ_c; hence, χ can only be calculated if τ_c is determined by some other method.

Far from extreme narrowing conditions ($\omega_0 \tau_c \gg 1$) For half-integer quadrupolar nuclei in the limit of slow isotropic molecular motion, as is the case for moderate to high frequency nuclei (i.e. ^{27}Al) bound to large proteins (i.e. transferrins), quadrupolar relaxation theory predicts that the central ($m_I = \frac{1}{2} \to -\frac{1}{2}$) transition can give rise to a relatively narrow signal, while the peaks due to all other components are broadened beyond detectability. For half-integer quadrupolar nuclei ($I = n/2$, where $n = 3, 5, 7$), the linewidth for the central transition in this window of molecular motion is given by [66–69]

$$\Delta v_{1/2}(m_I = \tfrac{1}{2} \to -\tfrac{1}{2}) = k \, \frac{\chi^2}{v_0^2 \tau_c} \qquad \begin{array}{ll} I = \tfrac{3}{2}, & k = 2.0 \times 10^{-2} \quad (2a) \\[4pt] I = \tfrac{5}{2}, & k = 4.9 \times 10^{-3} \quad (2b) \\[4pt] I = \tfrac{7}{2}, & k = 2.5 \times 10^{-3} \quad (2c) \end{array}$$

Notice that the linewidth of this signal decreases with increasing τ_c, and that it is dependent on the resonance frequency ν_0 of the nucleus, which in turn is dependent on the external magnetic field B_0.

The fractional intensity f_n of this component (and for that matter all transitions, $m_I = n \leftrightarrow n + 1; n = 1, 2, \ldots, 2I + 1$) for any quadrupolar nucleus can be easily deduced from [70]

$$f_n = \frac{n(2I + 1 - n)}{4 + 16(I - 1) + 10(I - 1)(I - 2) + 4(I - 1)(I - 2)(I - 3)/3} \tag{3}$$

Hence, in the slow motion limit one should theoretically observe only 40%, 25.7%, or 19.0% of the signal for $I = \frac{3}{2}, \frac{5}{2}$, and $\frac{7}{2}$ nuclei respectively, compared with conditions in which all components are detected (i.e. extreme narrowing).

A second important property of the signal due to the central transition in the slow motion limit is that its chemical shift is also markedly field dependent. This so-called "second-order dynamic frequency shift" $\Delta\delta_d$, illustrated in Fig. 11, is an upfield shift whose magnitude decreases with increasing B_0 according to [69–72].

$$\Delta\delta_d = \delta_{obs} - \delta_i \; (m_I = \tfrac{1}{2} \to -\tfrac{1}{2}) = -k\frac{\chi^2}{\nu_0^2} \quad
\begin{aligned}
I &= \tfrac{3}{2}, \quad k = 2.5 \times 10^4 & (4a)\\
I &= \tfrac{5}{2}, \quad k = 6.0 \times 10^3 & (4b)\\
I &= \tfrac{7}{2}, \quad k = 2.5 \times 10^3 & (4c)
\end{aligned}$$

where δ_{obs} (ppm) and δ_i (ppm) are the observed and isotropic (i.e. in the absence of second-order effects) chemical shifts respectively. Hence, Eq. (4) suggests that for a half-integer nucleus under these conditions an increase in B_0 translates into a downfield shift in the signal corresponding to the central transition. Also, the coefficients in Eqs. (2) and (4) indicate that the magnitudes of the field-dependent changes in both $\Delta\nu_{1/2}$ and δ_{obs} are inversely proportional to the nuclear spin.

Taken together, these expressions reveal that physical information (i.e. χ, δ_i, and τ_c) for a quadrupolar nucleus bound to a very large molecule (such that $\omega_0\tau_c \gg 1$) may be obtained from the field dependence of the linewidth and chemical shift of its observed signal.
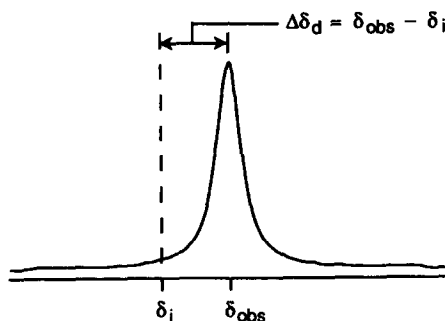

Fig. 11. Schematic diagram of the shift in the signal corresponding to the central transition of a quadrupolar nucleus when $\omega_0\tau_c \gg 1$ (Eq. (4)).

In addition to the above effects, Butler and Eckert [73] recently demonstrated for the first time that the effective 90° pulse length t_p for the central transition of a half-integer quadrupolar nucleus bound to a large molecule (transferrin-bound [51]V) is much shorter than that for the same nucleus under extreme narrowing conditions, in agreement with the following expression:

$$t_p(m_I = \tfrac{1}{2} \rightarrow -\tfrac{1}{2}) = \frac{t_p}{I + \tfrac{1}{2}} \tag{5}$$

This relation is valid when the r.f. pulse strength ω_1 is much less than the nuclear quadrupole coupling constant [74,75]. Pulse length effects are also extremely important in solid state NMR studies of such nuclei [76].

The quadrupole coupling constant χ in many of the above expressions reflects the magnitude of the coupling between the nuclear quadrupole moment eQ and the effective electric field gradient eq_{obs} at the nucleus and in frequency units (megahertz) is given by

$$\chi = \frac{e^2 Q q_{obs}}{h} \tag{6}$$

Hence, in the case of a complexed metal ion, the more symmetric the arrangement of ligands around the metal ion, the smaller the electric field gradient at the metal nucleus due to the ligands, and, thus, the smaller the value of χ.

From the above discussion, it is apparent that both the resonance position δ_{obs} and detectability $\Delta v_{1/2}$ of a quadrupolar nucleus in the limit of slow isotropic motion are dependent on a number of crucial intrinsic nuclear (I, Q, v_0), and molecular (eq_{ionic}, τ_c) properties, and on a key empirical variable (B_0).

2.7.3. Experiments with carbonate

In recent years we have successfully applied ^{27}Al NMR in tandem with ^{13}C NMR to monitor the binding of Al^{3+} to the high affinity Fe^{3+}-binding sites in transferrins. An example of this dual probe approach was given earlier for human sTf in the presence of carbonate (Fig. 6). In contrast to the ^{13}C NMR data for this experiment, the [27]Al signals due to the bound metal ion in the two sites of the protein are degenerate, and only one resonance slightly upfield of $Al(H_2O)_6^{3+}$ is detected ($B_0 =$ 9.4 T: $\delta = -5.4$ ppm, $\Delta v_{1/2} = 240$ Hz).

In the case of chicken OTf, one observes two [27]Al signals in the same region of the spectrum ($B_0 = 9.4$ T: $\delta = -4.6$ ppm, $\Delta v_{1/2} = 180$ Hz; $\delta = -6.8$ ppm; $\Delta v_{1/2} =$ 240 Hz) when two equivalents of Al^{3+} are added to the apoprotein in the presence of an excess of carbonate [51,52]. Similar to our ^{13}C NMR results, we found that Al^{3+} binding proceeds in a sequential manner, with the downfield resonance emerging on addition of one equivalent of metal ion, and the upfield signal appearing when further titrant is added. By plotting the areas of the [27]Al (and ^{13}C) signals corresponding to protein-bound Al^{3+} against number of equivalents of metal ion added, we have found that chicken OTf as well as human sTf and lTf in the presence of carbonate reach only 70%–80% saturation with Al^{3+} at the completion of the

titration [51,53]. Assignment of these signals using the proteolytic half-molecules of OTf (Fig. 12) provided conclusive evidence that Al^{3+} is bound preferentially at the *N*-terminal site of the protein when carbonate serves as the synergistic anion. At this point a very interesting observation was made. Notice that while the ^{13}C signals due to the bound anion in the isolated lobes are appreciably narrower than those in the native protein, the ^{27}Al signals for the half-molecules are significantly broader than the corresponding resonances in the intact protein (Table 5).

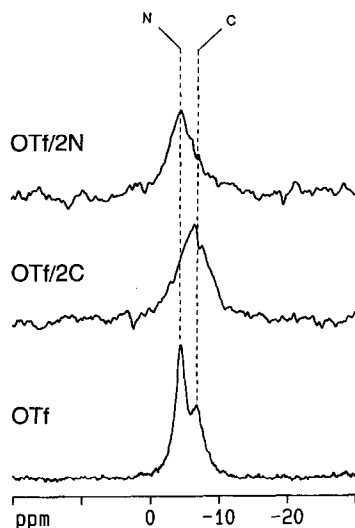Intuitively, one could argue that mild proteolysis of intact OTf perturbs the

Fig. 12. ^{27}Al (104.3 MHz) NMR spectra of the aluminum–carbonate derivatives of intact OTf and its half-molecules. OTf: 1.13 mM OTf, pH 7.6, 1.5×10^5 scans; OTf/2C: 0.30 mM OTf/2C, pH 7.7, 1.9×10^6 scans. OTf/2N: 0.19 mM OTf/2N, pH 7.6, 1.0×10^6 scans. (Reproduced with permission of the International Society of Magnetic Resonance from Ref. [52].)

Table 5
^{13}C and ^{27}Al nuclear magnetic resonance data for the $Al^{3+}–^{13}CO_3^{2-}$ adducts of chicken OTf, OTf/2N, and OTf/2C and human sTf and sTf/2N ($B_0 = 9.4$ T; 25°C)[a]

Protein	Site	^{13}C NMR		^{27}Al NMR	
		δ (ppm)	$\Delta v_{1/2}$ (Hz)	δ (ppm)	$\Delta v_{1/2}$ (Hz)
OTf	N	165.73	17	−4.6	180
	C	165.52	15	−6.8	240
OTf/2N	—	165.73	7	−4.6	410
OTf/2C	—	165.52	8	−6.5	460
sTf	C	166.16	18	−5.4	240
	N	165.83	19	−5.4	240
sTf/2N	—	165.80	9	−5.3	490

[a] Data obtained from Refs. [51–53].

structural integrity and metal ion binding activity of each lobe on the basis of the substantially larger ^{27}Al linewidths observed for the Al^{3+}-carbonate (and Al^{3+}-oxalate; vide infra) adducts of each of the half-molecules compared with the corresponding native proteins. However, this behavior can be explained by quadrupolar relaxation in the slow motion limit (Eq. (2)) and is due to a difference in the correlation times of the half-molecules vs. the intact proteins; this will be discussed in more detail in Section 2.7.6. We have obtained similar results for human sTf and its recombinant N-lobe; these data are also given in Table 5.

^{27}Al NMR spectra at a field of 11.7 T for the Al^{3+}-carbonate forms of transferrins from a number of species are shown in Fig. 13. Notice that, with the exception of bovine lTf, the ^{27}Al signals for serotransferrins and lactoferrins are degenerate, whereas in both ovotransferrins the resonances are overlapping, yet discernible. Table 6 gives a complete list of the ^{27}Al NMR data for these species at this field; note that the chemical shifts of the protein-bound ^{27}Al signals are field dependent (see Section 2.7.6).

The chemical shifts of the ^{27}Al signals due to transferrin-bound Al^{3+} reported here fall well within a window ($\delta \approx 40$ to -46 ppm) that is diagnostic of six-coordinate (octahedral) Al^{3+} complexes [59]. This result is consistent with the reported X-ray structures of transferrins alluded to above. It will be shown in Section 2.7.6 that the resonance frequencies of the transferrin-bound ^{27}Al signals are dependent on the external magnetic field B_0; hence, chemical shift data at one field
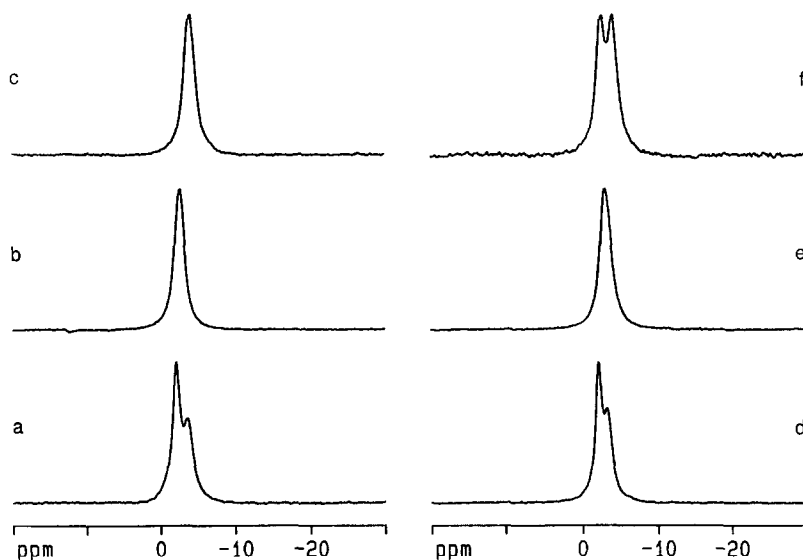

Fig. 13. ^{27}Al (130.3 MHz) NMR spectra of the aluminum–carbonate adducts of several transferrins: spectrum a, chicken OTf (1.13 mM, pH 7.5, 100 000 scans); spectrum b, human sTf (1.09 mM, pH 7.3, 10 000 scans); spectrum c, human lTf (0.73 mM, pH 7.6, 150 000 scans); spectrum d, turkey OTf (1.1 mM, pH 7.6, 100 000 scans); spectrum e, bovine sTf (1.2 mM, pH 7.5, 150 000 scans); spectrum f, bovine lTf (0.38 mM, pH 7.6, 500 000 scans). (From Refs. [57,63].)

Table 6
^{27}Al nuclear magnetic resonance data for the Al^{3+}–carbonate forms of various transferrins at 11.7 T and 25°C [a]

Protein	^{27}Al δ (ppm)	$\Delta v_{1/2}$ (Hz)	Site
Chicken OTf	−2.3	140	N
	−3·8	170	C
Chicken OTf/2N	−2.3	270	—
Chicken OTf/2C	−3.7	300	—
Human sTf	−2.8	180	N, C
Human sTf/2N	−2.8	320	—
Human lTf	−4.3	200	N, C
Turkey OTf	−2.2	110	n.d.
	−3.4	150	n.d.
Bovine sTf	−3.2	180	N, C
Bovine lTf	−2.8	170	n.d.
	−4.2	170	n.d.

[a] Data obtained from Refs. [57,63].

for such systems must be interpreted with caution. However, we will see that the isotropic chemical shifts δ_i of these resonances also conform with the data for octahedral aluminum.

The ^{27}Al NMR spectra shown in this section represent the first successful attempts to monitor directly Al^{3+} binding to transferrins by NMR. Recently, Fatemi et al. [62] failed to observe Al^{3+} bound to human sTf using this technique. However, it is possible that these workers may have missed the transferrin-bound ^{27}Al signal in their investigations because they neglected to consider its marked pulse angle dependence (i.e. 90° pulses were used; see Section 2.7.8) and did not eliminate the broad and intense background aluminum signal.

2.7.4. Experiments with oxalate

When Al^{3+} binds to chicken OTf in the presence of oxalate, two closely spaced ^{27}Al signals upfield of and significantly broader than those observed when carbonate serves as the synergistic anion ($B_0 = 9.4$ T: $\delta = -7.7$ ppm, $\Delta v_{1/2} = 240$ Hz; $\delta = -9.7$ ppm; $\Delta v_{1/2} = 310$ Hz) are observed [51]. Again, a site preference was noted in titration experiments; this time the more upfield resonance is predominantly observed when the first equivalent of metal ion is added. Unlike the carbonate results, we found that the areas of both the ^{13}C and the ^{27}Al NMR signals resulting from the complexation of Al^{3+} and oxalate at each site of OTf increase linearly up to two equivalents of metal ion, with no further changes at higher concentrations of the metal ion [51]. Thus, the protein is fully saturated with Al^{3+} at the end of the titration.

The half-molecule approach also affords the assignment of the ^{27}Al peaks to bound Al^{3+} in the N- and C-terminal sites of the protein (Fig. 14 [53]). For the Al^{3+}-oxalate form of each half-molecule, one observes signals at the same chemical shifts but with larger linewidths for Al^{3+} bound to the proteolytic fragments compared with the
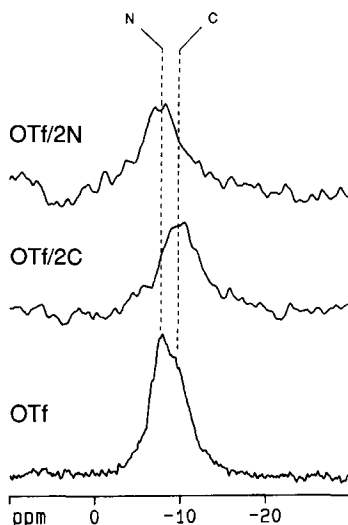
Fig. 14. ^{27}Al (104.3 MHz) NMR spectra of the aluminum–oxalate derivatives of intact OTf and its half-molecules. OTf: 1.18 mM OTf, pH 7.5, 1.5×10^5 scans. OTf/2C: 0.30 mM OTf/2C, pH 7.5, 2.9×10^6 scans. OTf/2N: 0.15 mM OTf/2N, pH 7.5, 1.3×10^6 scans. [53].

parent molecule ($B_0 = 9.4$ T: OTf/2N, $\delta = -7.8$ ppm, $\Delta v_{1/2} = 480$ Hz; OTf/2C, $\delta = -9.6$ ppm; $\Delta v_{1/2} = 520$ Hz). Furthermore, from these assignments and titration experiments we concluded that Al^{3+} complexation occurs preferentially at the C-site of OTf when oxalate is present, in contrast to what is observed for carbonate.

2.7.5. Competition experiments

The dual-probe methodology introduced in previous sections can be used to gain further insight into the Al^{3+} binding properties of transferrins. Here, this will be exemplified by competition experiments with Desferal®.

Desferal (DFO) is the mesylate derivative of a siderophore, desferrioxamine, native to *Streptomyces pilosus* (Fig. 15). This chelator binds Fe^{3+} and Al^{3+} with tremendous ferocity ($K_D \approx 10^{-31}$ and 10^{-22} M respectively) and has been used for decades as a therapeutic drug in the treatment of transfusional and thalassemic iron overload (for a recent review see Ref. [77]). DFO has also been used clinically for the removal of
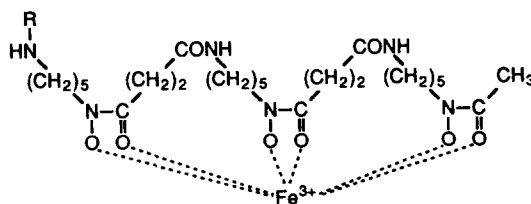

Fig. 15. Schematic drawing of the Fe^{3+} complex of desferrioxamine (R = H) and Desferal® (R = OSO_2CH_3).

Al^{3+} in renal dialysis patients [78], and recent evidence suggests that this drug retards progressive neurological degeneration in Alzheimer's patients [79]. In transferrin chemistry, DFO has been employed to generate a monoferric adduct of human sTf by selectively removing Fe^{3+} from the *C*-terminal site of the diferric protein [37]. When the $Al^{3+}–^{13}CO_3^{2-}$ derivative of OTf is titrated with DFO, both ^{13}C and ^{27}Al NMR clearly indicate that the metal ion is first extracted from the C-site of the protein, followed by the N-site (Fig. 16); the Al^{3+}–DFO complex is characterized by a ^{27}Al signal at $\delta = 32$ ppm, $\Delta v_{1/2} \approx 1$ kHz (not shown).

One can use this methodology to compare the affinity of Al^{3+} for transferrins with that for other metal ions. For example, when the aluminum–carbonate adduct of OTf is back titrated with Fe^{3+} the metal ion is again expelled from sites of the protein in a sequential manner (C first, then N [57]). Using this approach, we have found that Al^{3+} can be displaced from the sites of OTf by Ga^{3+}, Sc^{3+}, and Fe^{3+}, and binds to the protein more tightly than VO_2^+ [57].

2.7.6. Field dependence of transferrin-bound ^{27}Al signals

The results in Sections 2.7.3–2.7.5 demonstrate the feasibility of using quadrupolar (^{27}Al) NMR to probe metal ion (Al^{3+}) binding to larger proteins, such as transferrins.
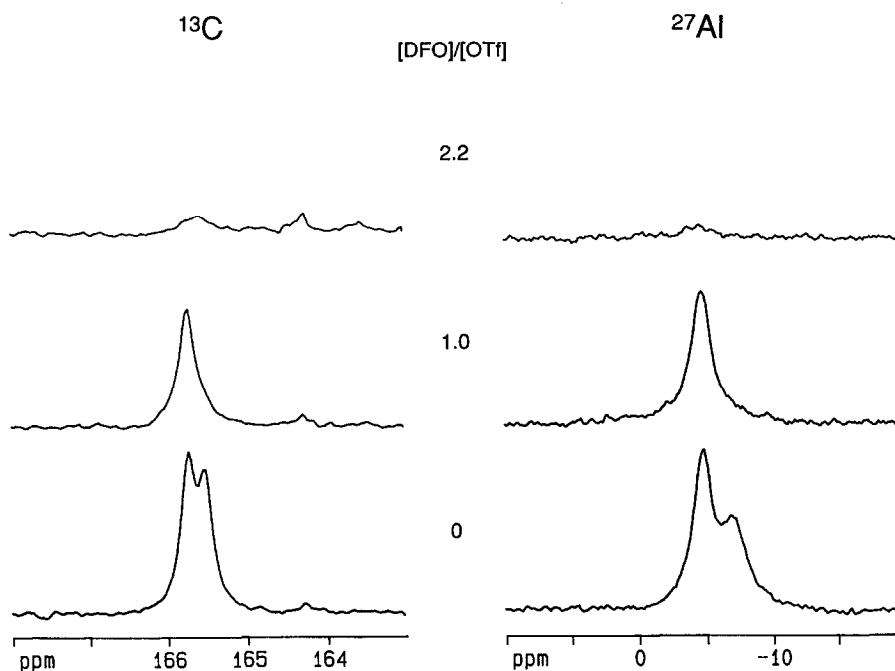

Fig. 16. ^{13}C (100.6 MHz) and ^{27}Al (104.3 MHz) NMR spectra of the Al^{3+}-carbonate form of OTf (1.19 mM, pH 7.6) plus various amounts of DFO. ^{13}C: 20 000 scans each; only the carbonyl region of each spectrum is shown. ^{27}Al: 150 000 scans each. (Reproduced with permission of the International Society of Magnetic Resonance from Ref. [52].)

The transferrin-bound ^{27}Al signals exhibit a number of peculiar properties that are characteristic of quadrupolar relaxation in a window of molecular motion that is well outside the extreme narrowing limit. These phenomena will be the focus of the next three sections.

Without question, the most critical trait of the ^{27}Al signals due to transferrin-bound Al^{3+} is the field dependence of their chemical shifts and linewidths. This is illustrated in Fig. 17, which shows ^{27}Al NMR spectra of the Al^{3+}/C$_2$O$_4^{2-}$ form of OTf [51] and the Al^{3+}–CO$_3^{2-}$ derivative of sTf/2N [53] at two magnetic fields ($B_0 = 9.4$ and 11.7 T). For each signal, increasing B_0 causes a downfield shift in peak position and a decrease in linewidth. Identical effects have been observed with each of the transferrins analyzed. These trends are in agreement with Eqs. (2) and (4) and are characteristic of the $m_I = \frac{1}{2} \rightarrow -\frac{1}{2}$ nuclei ($n = 3, 5, 7$) in the limit of slow molecular motion. Such effects are in stark contrast to the behavior of quadrupolar nuclei in other windows of molecular motion. For example, in extreme narrowing conditions both the chemical shift and linewidth of such nuclei are independent of field, and the latter is proportional to τ_c (Eq. (1)). Also, the chemical shifts of the corresponding ^{13}C signals for these and the other transferrins shown in Section 2.6 are not dependent on B_0.

By plotting the chemical shift and linewidth of each protein-bound ^{27}Al signal against the inverse of the square of the nuclear resonance frequency, as shown in
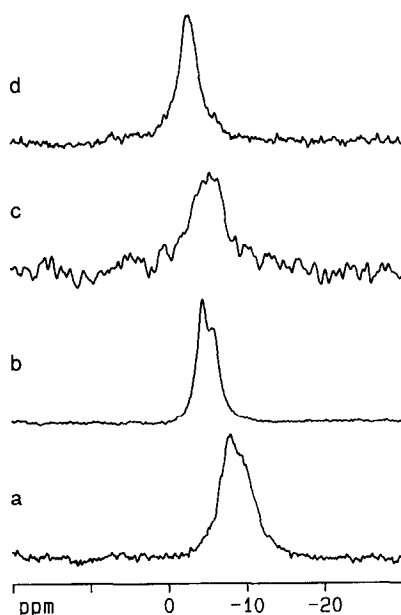

Fig. 17. ^{27}Al NMR spectra of the Al^{3+}–^{13}C$_2$O$_4^{2-}$ and Al^{3+}–^{13}CO$_3^{2-}$ forms of OTf and sTf/2N respectively at two magnetic fields: spectrum a, 1.18 mM OTf, pH 7.5, $B_0 = 9.4$ T, 1.5×10^5 scans; spectrum b, sample of spectrum a at $B_0 = 11.7$ T, 1.0×10^5 scans; spectrum c, 0.22 mM sTf/2N, pH 7.6, $B_0 = 9.4$ T, 2.1×10^6 scans; spectrum d, sample of spectrum c at $B_0 = 11.7$ T, 1.3×10^6 scans. (From Refs. [51,53].)

Fig. 18 for the Al^{3+}–CO_3^{2-} form of chicken OTf at five magnetic fields [63,64], we have obtained values of χ, δ_i, anad τ_c for Al^{3+} bound to several transferrins. A value for χ can be calculated from the slopes of two lines in Fig. 18 (full symbols) using Eq. (4b). The y intercepts of these curves give the unshifted (isotropic) chemical shifts δ_i of the bound ^{27}Al signals in these proteins ($\zeta_i \approx 1$–2.5 ppm), which fall well within the chemical shift window diagnostic of octahedral Al^{3+} [59a]. With these χ values in hand, the correlation time τ_c of the bound metal ion in each site can then be computed from the field dependence of the linewidth of each signal (open symbols) using Eq. (2b). Notice that the slopes of the curves for the half-molecules are significantly larger than those for the intact proteins, translating into much smaller values of τ_c for the proteolytic fragments. A complete list of the ^{27}Al NMR data obtained in this fashion for all of the transferrins analyzed in our laboratory is shown in Table 7.

The ^{27}Al values for Al^{3+} bound to the metal ion binding sites of each protein obtained with this approach range from 3.3 to 4.5 MHz. These numbers are comparable with results obtained on a model aluminum complex, tris-(2,4-pentanedionato)-aluminum ($Al(acac)_3$), in which six oxygen atoms form a near-perfect octahedral ligand coordination sphere about the central metal ion ($\chi = 3.1$ MHz [63,80]). This suggests a relatively high degree of symmetry for the metal ion in the sites of each protein, a notion supported by the recent X-ray crystallographic studies of a number of transferrins mentioned earlier. In addition, the ^{27}Al χ data indicate that the symmetry of metal ion sites in these proteins decreases in a series from one of the sites in turkey OTf ($\chi = 3.3$ MHz; most symmetric) to the C-site of chicken OTf with oxalate as the synergistic anion ($\chi = 4.5$ MHz; least symmetric).

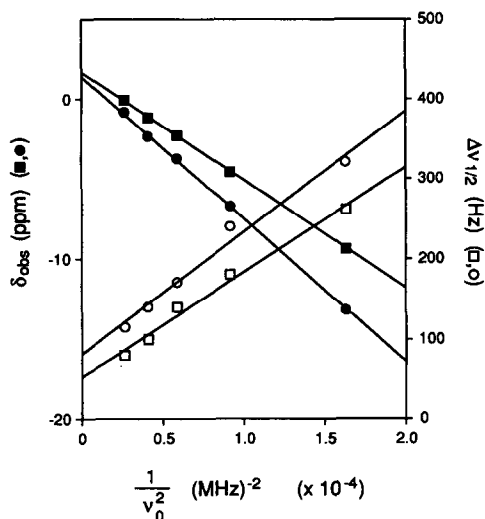The comparable values for the isotropic ^{27}Al chemical shifts δ_i for all transferrins

Fig. 18. Field dependence of the chemical shifts ($\blacksquare$, $\bullet$) and linewidths ($\square$, $\bigcirc$) of the ^{27}Al signals due to the Al^{3+}–$^{13}CO_3^{2-}$ form of OTf at five magnetic fields $B_0 = 7.0$, 9.4, 11.7, 14.1, and 17.6 T [63,64]. $\blacksquare$, $\square$ data for the N-sites; $\bullet$, $\bigcirc$ data for the C-sites.

Table 7
^{27}Al nuclear magnetic resonance χ, δ_i, and τ_c data for various transferrins (25°C)[a]

Protein	Anion	Site	χ (MHz)	δ_i (ppm)	τ_c (ns)
Chicken OTf	CO_3^{2-}	N	3.4	1.6	43
	CO_3^{2-}	C	3.9	1.4	48
Chicken OTf/2N	CO_3^{2-}	–	3.3	1.6	14
Chicken OTf/2C	CO_3^{2-}	—	3.7	1.1	17
Human sTf	CO_3^{2-}	N, C	3.6	1.7	58
Human sTf/2N	CO_3^{2-}	—	3.6	1.7	12
Human lTf	CO_3^{2-}	N, C	4.1	1.6	44
Turkey OTf	CO_3^{2-}	n.d.	3.3	1.7	35
	CO_3^{2-}	n.d.	3.8	1.6	33
Bovine sTf	CO_3^{2-}	N, C	3.8	1.8	29
Bovine lTf	CO_3^{2-}	n.d.	3.9	2.6	27
	CO_3^{2-}	n.d.	4.2	2.0	22
Chicken OTf	$C_2O_4^{2-}$	N	4.1	1.6	39
		C	4.5	1.4	30

[a] Data obtained from Refs. [57,63,64].

suggest that the differences in δ_{obs} at any field are primarily due to differences in χ (i.e. ligand geometry), rather than the chemical nature of the ligands coordinating the aluminum ion. This is a reasonable postulate given that the immediate coordination sphere of the bound metal ion is identical in the Fe^{3+}-binding sites of all transferrins. Note that the values of χ for Al^{3+} in the half-molecules of OTf and the corresponding sites in the intact protein are virtually identical, further suggesting that proteolysis of the loop that connects the two lobes of the protein does not alter the physical integrity of the metal ion binding sites in the isolated halves.

The correlation times for Al^{3+} in intact transferrins ($\tau_c \approx$ 30–50 ns) are significantly longer than those for the half-molecules of OTf and sTf ($\tau_c \approx$ 12–17 ns). These results are in good agreement with a recently published value for the τ_c of OTf (about 33 ns) obtained by perturbed angular correlation techniques [81], indicating that the bound Al^{3+} ions do not move with respect to the protein. In addition, the τ_c data account for the much larger linewidths of the ^{27}Al signals for the half-molecules compared with native OTf and sTf, also predicted by quadrupolar relaxation theory and in agreement with the ^{13}C NMR linewidth data (vide infra; Table 5). These results indicate that the motions of the lobes in the intact protein are restricted, a characteristic that is quite different from other bilobal proteins, such as the dumb-bell shaped Ca^{2+}-binding protein calmodulin, where the correlation times of the isolated half-molecules and the native proteins are virtually identical [82].

One footnote to this field dependence work should be mentioned. In contrast to the behavior of the protein-bound ^{27}Al signals, ^{13}C NMR studies of the Al^{3+}–$^{13}CO_3^{2-}$ adduct of OTf acquired at the same four magnetic fields reveal that the linewidths of the ^{13}C peaks due to the bound anion in each site of the protein increase with increasing B_0 (i.e. from about 10 Hz at a $B_0 = 7.0$ T to about 30 Hz at a field of 14.1 T [57]). In fact, if one plots the ^{13}C data against the square of the

magnetic field it is evident that at higher fields the chemical shift anisotropy mechanism [83] becomes the most important relaxation pathway for these nuclei, a result expected for non-protonated carbon atoms.

2.7.7. OTf half-molecule reassociation experiments

As we have shown in previous sections, the linewidths of transferrin-bound ^{27}Al signals are markedly dependent on the correlation time of the protein. In this section we describe how this behavior can be exploited to examine the reassociation of the proteolytic half-molecules of OTf.

In recent years, several lines of evidence have established that the tryptic *N*- and *C*-terminal half-molecules of OTf can associate in solution in a non-covalent fashion, with a dissociation constant in the micromolar range or lower [29,84,85]. Williams and Moreton [86] showed that these interactions are localized to α-helices at the *C*-terminal ends of both lobes (residues 321–332 and 675–686), analogous to the situation observed in the crystal structure of intact lTf [7]. It is widely believed that the interlobal interactions in native transferrins have physiological implications, providing the correct molecular orientation necessary for receptor recognition. This is exemplified by the receptor binding studies of Brown-Mason and Woodworth [87], which revealed that equimolar mixtures of the proteolytic fragments of OTf deliver Fe^{3+} to cells with an efficacy rivalling that of the intact protein, whereas this activity is negligible for the isolated half-molecules. Recent studies involving monoclonal antibodies specific to either the *N*- or *C*-lobes in the intact protein or the isolated *N*-terminal half-molecule corroborate this view [88].

Fig. 19 shows ^{27}Al NMR spectra of the Al^{3+}-carbonate forms of the *N*- and *C*-terminal half-molecules of OTf (spectra a and b), the reassociation of these half-molecules (spectra c and d), and intact OTf (spectrum e) [89]. When 0.5 equivalent of the *N*-terminal fragment is added to a sample containing the *C*-terminal half-molecule one obtains a spectrum that can be fitted to three signals; a broad resonance at $\delta = -3.8$ ppm ($\Delta v_{1/2} = 310$ Hz) due to the excess C-half and two narrower signals at $\delta = -2.2$ and -3.7 ppm corresponding to the reassociated halves (Fig. 19, spectrum c). The presence of both the reassociated and the free forms of the C-lobe is indicative of slow exchange and is consistent with the tight binding reported in previous studies of this dimerization. Also, in the absence of reassociation, one would expect simply to observe two broad signals corresponding to the isolated lobes in a 1:2 ratio at this point in the titration. When the two half-molecules are present in equimolar amounts one obtains a spectrum consisting of two signals with chemical shifts and linewidths comparable with the resonances observed for bound Al^{3+} in the intact protein (Fig. 19). The empirical results are in good agreement with calculated spectra, in which half-molecule reassociation is assumed [89]. The ^{27}Al NMR data for the isolated half-molecules, intact OTf, and the reassociation experiment are presented in Table 8. Analogous effects were observed for the complementary experiment (i.e. N titrated with C; data not shown).

We have found that other experimental variables that alter the correlation time of the protein, such as temperature and viscosity, also have a marked effect on the linewidths of transferrin-bound ^{27}Al NMR resonances. In particular, changes that
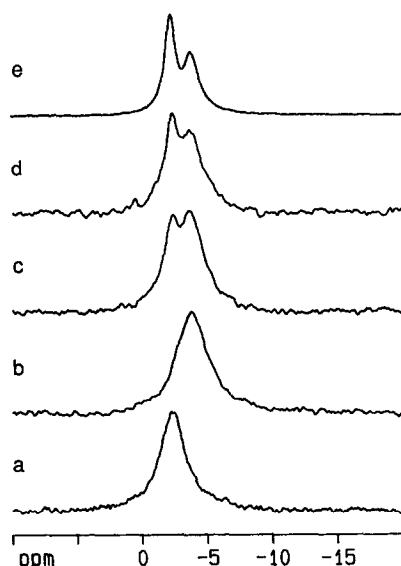
Fig. 19. ^{27}Al NMR (130.3 MHz) spectra at 25°C of the Al^{3+}–$^{13}CO_3^{2-}$ forms of OTf/2N (0.14 mM, pH 7.6, 1×10^6 scans (spectrum a), OTf/2C (0.15 mM, pH 7.7) (spectrum b), OTf/2C (0.15 mM, pH 7.6) + 0.5 equivalents of OTf/2N (1×10^6 scans) (spectrum c), sample of spectrum c plus an additional 0.5 equivalents of OTf/2N (6×10^5 scans) (spectrum d), and OTf (0.95 mM, pH 7.7, 1.5×10^5 scans) (spectrum e). (From Ref. [89].)

Table 8
^{27}Al nuclear magnetic resonance data for the reassociation of the Al^{3+}–carbonate forms of OTf/2N and OTf/2C [a]

Sample	δ (ppm)	$\Delta\nu_{1/2}$ (Hz)
OTf/2N	−2.3	270
OTf/2C	−3.7	300
Reassociated halves	−2.3	140
	−3.8	200
OTf	−2.3	130
	−3.8	170

[a] The data shown for the reassociated halves are averages of the results obtained for OTf/2C + OTf/2N and OTf/2N + OTf/2C experiments.

result in an increase in molecular correlation time (i.e. decreasing temperature and increasing viscosity) result in a decrease in signal linewidth, in accordance with the behavior of the central transition of a quadrupolar nucleus when $\omega_0 \tau_c \gg 1$ predicted by quadrupolar relaxation theory (Eq. (2)) [89]. Such effects have also been documented for other quadrupolar metal nuclei bound to transferrins (i.e. ^{45}Sc [55]).

2.7.8. Pulse angle dependence of transferrin-bound ^{27}Al signals

The intensities of the protein-bound ^{27}Al NMR signals exhibit a rather peculiar dependence on the length of the transmitter pulse. Plots of the integrated ^{27}Al NMR signal area as a function of pulse length for samples of free aluminum (i.e. $Al(H_2O)_6^{3+}$) and the Al^{3+}–$^{13}CO_3^{2-}$ forms of OTf, sTf, and lTf containing an equimolar amount of Al^{3+} are shown in Fig. 20. Two differences between the data for the metal ion in these environments (i.e. free and protein bound) are clearly noticeable. First, the area of each Al^{3+}-transferrin signal reaches a maximum at a pulse length (about 8 µs) that is appreciably less than that of the 90° pulse for aqueous Al^{3+} (18 µs). Second, the areas of the protein-bound ^{27}Al signals are significantly less than the area obtained for the free metal ion over virtually the entire spectrum of pulse lengths examined. In fact, for each transferrin, the maximum area for the ^{27}Al signal is only about 15%–20% of that for free Al^{3+} at the same flip angle (about 40°). We have obtained virtually identical results for Al^{3+} adducts of other transferrins [57].

The strange pulse length effects observed for the transferrin-bound ^{27}Al signal mirror the ^{51}V NMR results for sTf reported by Butler and Eckert [73]. The substantially lower signal areas of transferrin-bound Al^{3+} compared with the free metal ion add further credence to the idea that only the central component of the bound quadrupolar nucleus is detected. For small flip angles (i.e. up to about 40°) this area is about 15%–20% that for free Al^{3+}, which is comparable with the theoretically predicted limit (25.7%) for the contribution of this component to the signal area of an $I = \frac{5}{2}$ nucleus when $\omega_0 \tau_c \gg 1$ (Eq. (3)). In addition, the protein-bound ^{27}Al signal area peaks at a pulse length corresponding to a ca. 40° pulse for
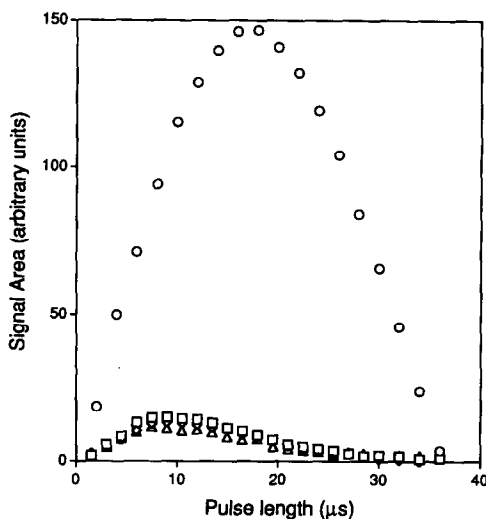

Fig. 20. Pulse length dependence of the integrated ^{27}Al NMR (104.3 MHz) signal areas of 1.00 mM $Al(NO_3)_3$ (○), and the Al^{3+}–$^{13}CO_3^{2-}$ forms of OTf (1.00 mM, 1.0 equivalents Al^{3+}) □), sTf (1.00 mM, 1.0 equivalents Al^{3+}) (◇), and lTf (0.73 mM, 1.5 equivalents Al^{3+}) (△). A total of 50 000 scans were acquired in each experiment, and an r.f. strength (ω_1) of 13.9 kHz was used throughout. (From Refs. [51,53].)

free Al^{3+}. However, no negative signals are observed up to a flip angle of 180°, suggesting that the outer components may also be partially excited under these conditions [73]. One would think that attenuating the power of the applied r.f. pulse (ω_1) should increase the selectivity of the excitation of the central component and, in principle, shift the effective 90° pulse length toward the predicted value (30°; Eq. (6)). Such phenomena have been reported (i.e. for ^{23}Na), and the flip angle effect has been touted as a useful technique for determining the motional characteristics of quadrupolar metal ions in tissues [90].

3. Conclusions and future prospects

The recent spectroscopic studies of the transferrins reviewed in this paper reveal a number of interesting facets pertaining to the physiologically relevant Al^{3+} forms of these proteins. The X-ray solution scattering work indicates that Al^{3+} binding to transferrins causes conformational changes that are distinct from those found with other metal ions. The other approaches, in particular the NMR studies, reveal subtle differences in the metal ion binding and/or anion binding sites within the same protein and among a series of transferrins. Also, the relative Al^{3+} affinities of sites in the same protein can be altered by changing the synergistic anion (i.e. for chicken OTf) or the amount of salt in the sample (i.e. for human sTf).

The ^{27}Al NMR studies of the transferrins demonstrate that quadrupolar metal ion NMR can be a unique means of gaining insight into the symmetry of metal binding sites and the motions of bound metal ions in such large metalloproteins. From field-dependent chemical shift and linewidth information one can determine the quadrupole coupling constant χ, isotropic chemical shift δ_i, and rotational correlation time τ_c of the bound metal ion in these proteins. This work also demonstrates that transferrin-bound ^{27}Al signals possess a number of unique traits, all of which are predicted by quadrupolar relaxation theory as being intrinsic to the central ($m_I = \frac{1}{2} \rightarrow -\frac{1}{2}$) transition of a quadrupolar nucleus in the limit of slow isotropic molecular motion. As well as providing physical information about the metal ion binding sites in large metalloproteins, these phenomena provide the basis for understanding the conditions and experimental parameters (i.e. magnetic field, temperature, viscosity, pulse length) which may facilitate the application of this "quadrupolar central transition" approach to the study of other quadrupolar nuclei and proteins. Since the majority of NMR nuclei in the periodic table share most of the quadrupolar properties of ^{27}Al, this approach may be suitable for a broad spectrum of biological applications. Also, the advent of very high field NMR spectrometers will further facilitate quadrupolar metal ion and high resolution ^1H NMR studies of large metalloproteins such as the transferrins.

Acknowledgements

Note added in proof

Following the acceptance of this manuscript for publication, several relevant publications regarding aluminum binding to transferrins have appeared. We will briefly summarize those here. The role of transferrin and small chelators such as citrate and phosphate for the binding of Al^{3+} in serum has been re-evaluated leading to the conclusion that $\approx 89\%$ of Al^{3+} in serum is bound to transferrin and $\sim 11\%$ to citrate [91]; these results underscore the clinical relevance of studying this protein–Al^{3+} binding event. Also, optical spectroscopy techniques such as circular dichroism (CD) and fluorescence spectroscopy have now been used to study this interaction [48,92]. The far-ultraviolet CD spectra of serum transferrin were not sensitive to the binding of Al^{3+}, Ga^{3+}, or In^{3+} [48], or showed only small changes [92], ruling out major alterations in the secondary structure of the protein during metal ion binding [48]. However, changes were observed in the near-UV region, indicating changes in the environment for several aromatic sidechains in a metal ion dependent manner [48,92]. Fluorescence studies provided further proof that in addition to the tyrosine residues involved directly in liganding Al^{3+}, several tryptophan residues in the vicinity of the metal ion binding sites were also affected [92]. Using small angle X-ray scattering, Castellano et al. [93] compared Fe_2-sTf and Al_2-sTf at two different pH values. Their work has shown that pH may play a critical role in the conformation of the open or closed state of the protein, more so than the type of metal ion bound. Finally, relevant to the work described here earlier on oxalate binding to transferrins, a recent study utilizing isoelectric focussing (iEF) has shown that the aluminum–oxalate–transferrin complex is more stable than its carbonate counterpart [94]. The authors went on to suggest that this complex may have a significant function in vivo. In summary, these recent publications have all indicated that the binding of Al^{3+} to transferrin does not induce the same conformational changes as iron, but that it does affect the nature of the overall protein conformation. As discussed in this review, this overall conformation change is attributed to the smaller size of the Al^{3+} ion and the possible inability of the site to close fully over the metal ion. Further definitive studies will be needed to determine conclusively whether this small conformational difference affects the binding of Al_2-sTf to its receptors, and ultimately controls the distribution of Al^{3+} in vivo.

References

[1] (a) E.N. Baker and P.F. Lindley, J. Inorg. Biochem., 47 (1992) 147–160. (b) G. de Jong, J.P. van Dijk and H.G. van Eijk, Clin. Chim. Acta, 190 (1990) 1–46. (c) D.C. Harris and P. Aisen, in T.M. Loehr (Ed.), Physical Bioinorganic Chemistry, Vol. 5, VCH, New York, 1989, pp. 239–351. (d) H.A. Heubers and C.A. Finch, Physiol. Rev., 67 (1987) 520–582. (e) J.H. Brock, in P.M. Harrison (Ed.), Metalloproteins, Part 2, Macmillan, London, 1985, pp. 183–262.

[2] M.-H. Metz-Boutigue, J. Jollès, J. Mazurier, F. Schoentgen, D. Legrand, G. Spik, J. Montreuil and P. Jollès, Eur. J. Biochem., 145 (1984) 659–676.

[3] I. Park, E. Schaeffer, A. Sidoli, F.E. Baralle, G.N. Cohen and M.N. Zakin, Proc. Natl. Acad. Sci. USA, 82 (1985) 3149–3153.

[4] M.R. Schlabach and G.W. Bates, J. Biol. Chem., 250 (1975) 2182–2188.

[5] C. Luchinat and M. Sola, in Encyclopedia of NMR, in press.

[6] B.F. Anderson, H.M. Baker, E.J. Dodson, G.E. Norris, S.V. Rumball, J.M. Waters and E.N. Baker, Proc. Natl. Acad. Sci. USA, 84 (1987) 1769–1773.

[7] B.F. Anderson, H.M. Baker, G.E. Norris, D.W. Rice and E.N. Baker, J. Mol. Biol., 209 (1989) 711–734.

[8] C.L. Day, B.F. Anderson, J.W. Tweedie and E.N. Baker, J. Mol. Biol., 232 (1993) 1084–1100.

[9] E.N. Baker, S.V. Rumball and B.F. Anderson, Trends Biochem. Sci., 12 (1987) 350–353.

[10] S. Bailey, R.W. Evans, R.C. Garratt, B. Gorinsky, S. Hasnain, C. Horsburgh, H. Jhoti, P.F. Lindley, A. Mydin, R. Sarra and J.L. Watson, Biochemistry, 27 (1988) 5804–5812.

[11] R. Sarra, R. Garratt, B. Gorinsky, H. Jhoti and P. Lindley, Acta Crystallogr. B, 46 (1990) 763–771.

[12] J.C. Dewan, B. Mikami, M. Hirose and J.C. Sacchettini, Biochemistry, 32 (1993) 11963–11968.

[13] B.F. Anderson, H.M. Baker, G.E. Norris, S.V. Rumball and E.N. Baker, Nature (London), 344 (1990) 784–787.

[14] M. Gerstein, B.F. Anderson, G.E. Norris, E.N. Baker, A.M. Lesk and C. Chothia, J. Mol. Biol., 234 (1993) 357–372.

[15] J.G. Grossmann, M. Neu, E. Pantos, F.J. Schwab, R.W. Evans, E. Towne-Andrews, P.F. Lindley, H. Appel, W.-G. Thies and S.S. Hasnain, J. Mol. Biol., 225 (1992) 811–819.

[16] J.G. Grossmann, M. Neu, R.W. Evans, P.F. Lindley, H. Appel and S.S. Hasnain, J. Mol. Biol., 229 (1993) 585–590.

[17] J.G. Grossmann, A.B. Mason, R.C. Woodworth, M. Neu, P.F. Lindley and S.S. Hasnain, J. Mol. Biol., 231 (1993) 554–558.

[18] C.A. Smith, H.M. Baker and E.N. Baker, J. Mol. Biol., 219 (1991) 155–159.

[19] M.S. Shongwe, C.A. Smith, E.W. Ainscough, H.M. Baker, A.M. Brodie and E.N. Baker, Biochemistry, 31 (1992) 4451–4458.

[20] P.F. Lindley, M. Bajaj, R.W. Evans, R.C. Garratt, S.S. Hasnain, H. Jhoti, P. Kuser, M. Neu, K. Patel, R. Sarra, R. Strange and A. Walton, Acta Crystallogr. D, 49 (1993) 292–304.

[21] (a) D.J. Chadwick and J. Whelan (Eds.), Aluminum in Biology and Medicine, CIBA Foundation Symposium 169, Wiley, Chichester, 1992. (b) H. Sigel (Ed.), Metal Ions in Biological Systems, Vol. 24, Dekker, New York, 1988.

[22] G. Farrar, P. Altmann, S. Welch, O. Wychrij, B. Ghose, J. Lejeune, J. Corbett, V. Prasher and J.A. Blair, Lancet, 335 (1990) 747–750.

[23] S.J. McGregor, D. Brown and J.H. Brock, Lancet, 338 (1991) 1394–1395.

[24] G.A. Taylor, C.M. Morris, A.F. Fairbairn, J.M. Candy and J.A. Edwardson, Lancet, 338 (1991) 1395–1396.

[25] J.P. Landsberg, B. McDonald and F. Watt, Nature (London), 360 (1992) 65–68.

[26] C. Exley, N.C. Price, S.M. Kelly and J.D. Birchall, FEBS Lett., 324 (1993) 293–295.

[27] G.E. Jackson, Polyhedron, 9 (1990) 163–170.

[28] R.D. Shannon, Acta Crystallogr. A, 32 (1976) 751–767.

[29] H. Oe, E. Doi and M. Hirose, J. Biochem. (Tokyo), 103 (1988) 1066–1072.

[30] K. Nakazato, I. Enami, Y. Tanaka, Y. Uchiyama, A. Tsugita and K. Satake, Biosci. Biotechnol. Biochem., 56 (1992) 687–688.

[31] J. Lineback-Zins and K. Brew, J. Biol. Chem., 255 (1980) 708–713.
[32] D. Legrand, J. Mazurier, J.-P. Aubert, M.-H. Loucheux-Lefebvre, J. Montreuil and G. Spik, Biochem. J., 236 (1986) 839–844.
[33] D.J. Thornton, D.F. Holmes, J.K. Sheehan and I. Carlstedt, Anal. Biochem., 182 (1989) 160–164.
[34] W.D. Funk, R.T.A. MacGillivray, A.B. Mason, S.A. Brown and R.C. Woodworth, Biochemistry, 29 (1990) 1654–1660.
[35] A.B. Mason, W.D. Funk, R.T.A. MacGillivray and R.C. Woodworth, Protein Expr. Purif., 2 (1991) 214–220.
[36] C.L. Day, K.M. Stowell, E.N. Baker and J.W. Tweedie, J. Biol. Chem., 267 (1992) 13857–13862.
[37] D.A. Folajtar and N.D. Chasteen, J. Am. Chem. Soc., 104 (1982) 5775–5780.
[38] D.A. Baldwin and D.M.R. de Sousa, Biochem. Biophys. Res. Commun., 99 (1981) 1101–1107.
[39] J.M. Aramini, P.H. Krygsman and H.J. Vogel, Biochemistry, 33 (1994) 3304–3311.
[40] W.R. Harris and J. Sheldon, Inorg. Chem., 29 (1990) 119–124.
[41] K. Ichimura, H. Kihara, T. Yamamura and K. Satake, J. Biochem. (Tokyo), 106 (1989) 50–54.
[42] R.B. Martin, J. Savory, S. Brown, R.L. Bertholf and M.R. Will, Clin. Chem., 33 (1987) 405–407.
[43] M. Cochran, J. Coates and S. Neoh, FEBS Lett., 176 (1984) 129–132.
[44] H. Durchschlag, P. Zipper, R. Wilfing and G. Purr, J. Appl. Crystallogr., 24 (1991) 822–831.
[45] S.P. Young, A. Bomford and R. Williams, Biochem. J., 219 (1984) 505–510.
[46] (a) G.C.K. Roberts (Ed.), NMR of Macromolecules; A Practical Approach, Oxford University Press, New York, 1993. (b) G.M. Clore and A.M. Gronenborn (Eds.), NMR of Proteins, CRC Press, Boca Raton, FL, 1993.
[47] (a) G. Kubal and P.J. Sadler, J. Am. Chem. Soc., 114 (1992) 1117–1118. (b) G. Kubal, A.B. Mason, P.J. Sadler, A. Tucker and R.C. Woodworth, Biochem. J., 285 (1992) 711–714.
[48] G. Battistuzi, L. Calzolai, L. Messori and M. Sola, Biochem. Biophys. Res. Commun., 206 (1998) 161–170.
[49] G. Kubal, A.B. Mason, S.U. Patel, P.J. Sadler and R.C. Woodworth, Biochemistry, 32 (1993) 3387–3395.
[50] I. Bertini, C. Luchinat, L. Messori, A. Scozzafava, G. Pellacani and M. Sola, Inorg. Chem., 25 (1986) 1782–1786.
[51] J.M. Aramini and H.J. Vogel, J. Am. Chem. Soc., 115 (1993) 245–252.
[52] J.M. Aramini and H.J. Vogel, Bull. Magn. Reson., 15 (1993) 84–88.
[53] J.M. Aramini and H.J. Vogel, unpublished results, 1994.
[54] J.L. Zweier, J.B. Wooten and J.S. Cohen, Biochemistry, 20 (1981) 3505–3510.
[55] J.M. Aramini and H.J. Vogel, J. Am. Chem. Soc., 116 (1994) 1988–1993.
[56] J.M. Aramini, D.D. McIntyre and H.J. Vogel, J. Am. Chem. Soc., 116 (1994) 11506–11511.
[57] J.A. Saponja, J.M. Aramini and H.J. Vogel, unpublished results, 1995.
[58] J. Dubach, B.J. Gaffney, K. More, G.R. Eaton and S.S. Eaton, Biophys. J., 59 (1991) 1091–1100.
[59] (a) J.W. Akitt, Prog. Nucl. Magn. Reson. Spectrosc., 21 (1989) 1–149. (b) J.W. Akitt, in J. Mason (Ed.), Multinuclear NMR, Plenum, New York, 1987, pp. 259–292. (c) J.J. Delpuech, in P. Laszlo (Ed.), NMR of Newly Accessible Nuclei, Vol. 2, Academic Press, New York, 1983, pp. 153–195.
[60] I. Mills, T. Cvitas, K. Homann, N. Kallay and K. Kuchitsu, Quantities, Units and Symbols in Physical Chemistry, Blackwell, Oxford, 2nd edn., 1993, pp. 98–104.
[61] C. Brevard and P. Granger, Handbook of High Resolution Multinuclear NMR, Wiley, New York, 1981.
[62] S.J.A. Fatemi, D.J. Williamson and G.R. Moore, J. Inorg. Biochem., 46 (1992) 35–40.
[63] J.M. Aramini, M.W. Germann and H.J. Vogel, J. Am. Chem. Soc., 115 (1993) 9750–9753.
[64] M.W. Germann, J.M. Aramini and H.J. Vogel, J. Am. Chem. Soc., 116 (1994) 6971–6972.
[65] A. Abragam, Principles of Nuclear Magnetism, Oxford University Press, Oxford, 1961.
[66] S. Forsén and B. Lindman, in D. Glick (Ed.), Methods of Biochemical Analysis, Vol. 27, Wiley, New York, 1981, pp. 289–486.
[67] P.S. Hubbard, J. Chem. Phys., 53 (1970) 985–987.
[68] T.E. Bull, S. Forsén and D.L. Turner, J. Chem. Phys., 70 (1979) 3106–3111.
[69] P.-O. Westlund and H. Wennerström, J. Magn. Reson., 50 (1982) 451–466.
[70] L.G. Werbelow, J. Chem. Phys., 70 (1979) 5381–5383.

[71] L.G. Werbelow and A.G. Marshall, J. Magn. Reson., 43 (1981) 443–449.
[72] L.G. Werbelow and G. Pouzard, J. Phys. Chem., 85 (1981) 3887–3891.
[73] (a) A. Butler and H. Eckert, J. Am. Chem. Soc., 111 (1989) 2802–2809. (b) J. Saponja and H.J. Vogel, J. Inorg. Biochem., 61 (1996) in press.
[74] S. Vega, J. Chem. Phys., 68 (1978) 5518–5527.
[75] A. Wokaun and R.R. Ernst, J. Chem. Phys., 67 (1977) 1752–1758.
[76] A. Samoson and E. Lippmaa, Phys. Rev. B, 28 (1983) 6567–6570.
[77] C. Hershko, Mol. Aspects Med., 13 (1992) 113–165.
[78] R.D. Swartz, Am. J. Kidney Dis., 6 (1985) 358–364.
[79] D.R.C. McLachlan, A.J. Dalton, T.P.A. Kruck, M.Y. Bell, W.L. Smith, W. Kalow and D.F. Andrews, Lancet, 337 (1991) 1304–1308.
[80] J.J. Dechter, U. Henricksson, J. Kowalewski and A.-C. Nilsson, J. Magn. Reson., 48 (1982) 503–511.
[81] F.J. Schwab, H. Appel, M. Neu and W.-G. Thies, Eur. Biophys. J., 21 (1992) 147–154.
[82] G. Barbato, M. Ikura, L.E. Kay, R.W. Pastor and A. Bax, Biochemistry, 31 (1992) 5269–5278.
[83] T.C. Farrar and E.D. Becker, Pulse and Fourier Transform NMR, Academic Press, New York, 1971.
[84] H. Ikeda, Y. Nabuchi, K. Nakazato, Y. Tanaka and K. Satake, FEBS Lett., 182 (1985) 305–309.
[85] A. Brown-Mason, S.A. Brown, N.D. Butcher and R.C. Woodworth, Biochem. J., 245 (1987) 103–109.
[86] J. Williams and K. Moreton, Biochem. J., 251 (1988) 849–855.
[87] A. Brown-Mason and R.C. Woodworth, J. Biol. Chem., 259 (1984) 1866–1873.
[88] A.B. Mason, S.A. Brown and W.R. Church, J. Biol. Chem., 262 (1987) 9011–9015.
[89] J.M. Aramini and H.J. Vogel, J. Magn. Reson. B, 110 (1996) 182–187.
[90] P.M. Joseph and R.M. Summers, Magn. Reson. Med., 4 (1987) 67–77.
[91] L.-O. Öhman and R.B. Martin, Clin. Chem., 40 (1994) 598–601.
[92] S. Tang, R. MacColl and P.J. Parsons, J. Inorg. Biochem., 60 (1995) 175–185.
[93] A.C. Castellano, M. Barteri, M. Castagnola, A. Bianconi, E. Borghi and S. Della Longa, Biochem. Biophys. Res. Commun., 198 (1994) 646–652.
[94] G. de Jong, C.C.A. Ammerlaan, W.L. van Noort, H.G. van Eijk, G.L. van Landeghem, P.C. D'Haese and M.E. de Broe, Biometals, 8 (1995) 352–356.